[O II] nebular emission from Mg II absorbers: star formation associated with the absorbing gas

Ravi Joshi, Raghunathan Srianand, Patrick Petitjean, Pasquier Noterdaeme

Monthly Notices of the ROYAL ASTRONOMICAL SOCIETY

MNRAS **471,** 1910–1925 (2017)
Advance Access publication 2017 June 16

doi:10.1093/mnras/stx1499

[O II] nebular emission from Mg II absorbers: star formation associated with the absorbing gas

Ravi Joshi,[1★] Raghunathan Srianand,[1] Patrick Petitjean[2] and Pasquier Noterdaeme[2]

[1] *Inter-University Centre for Astronomy and Astrophysics, Post Bag 4, Ganeshkhind, Pune 411007, India*
[2] *UPMC-CNRS, UMR7095, Institut d'Astrophysique de Paris, F-75014 Paris, France*

Accepted 2017 June 14. Received 2017 June 9; in original form 2017 January 5

ABSTRACT

We present nebular emission associated with 198 strong Mg II absorbers at $0.35 \leq z \leq 1.1$ in the fibre spectra of quasars from the Sloan Digital Sky Survey. Measured [O II] luminosities ($L_{[\rm O\,II]}$) are typical of sub-$L^{\star}$ galaxies with derived star formation rate (uncorrected for fibre losses and dust reddening) in the range of 0.5–20 $\rm M_{\odot}\ yr^{-1}$. Typically less than ∼3 per cent of the Mg II systems with rest equivalent width, $W_{2796}{\geq}2$Å, show $L_{[\rm O\,II]}\geq 0.3\,L^{\star}_{[\rm O\,II]}$. The detection rate is found to increase with increasing W_{2796} and z. No significant correlation is found between W_{2796} and $L_{[\rm O\,II]}$ even when we restrict the samples to narrow z ranges. A strong correlation is seen between $L_{[\rm O\,II]}$ and z. While this is expected from the luminosity evolution of galaxies, we show that finite fibre size plays a very crucial role in this correlation. The measured nebular line ratios (like [O III]/[O II] and [O III]/H β) and their z evolution are consistent with those of galaxies detected in deep surveys. Based on the median stacked spectra, we infer the average metallicity (log Z ∼8.3), ionization parameter (log q∼7.5) and stellar mass (log $(M/\rm M_{\odot})$ ∼ 9.3). The Mg II systems with nebular emission typically have W_{2796} ≥2 Å, Mg II doublet ratio close to 1 and W(Fe II λ2600)/W_{2796}∼0.5 as often seen in damped Ly α and 21-cm absorbers at these redshifts. This is the biggest reported sample of [O II] emission from Mg II absorbers at low-impact parameters ideally suited for probing various feedback processes at play in $z \leq 1$ galaxies.

Key words: galaxies: evolution – galaxies: ISM – quasars: absorption lines – galaxies: star formation – cosmology: observations.

1 INTRODUCTION

Absorption line systems traced by Mg II λλ2796, 2803 doublet in the quasar spectra provide a direct tracer of cool, $T \sim 10^4\,K$, gas within gaseous haloes and circumgalactic medium surrounding galaxies over a wide range of H I column densities, $16 \leq \log\,[N(\rm H\,I)\ cm^{-2}] \leq 22$ (Bergeron 1986; Churchill et al. 2000; Rao & Turnshek 2000; Rigby, Charlton & Churchill 2002), out to projected distances of ∼ 200 kpc (e.g. Kacprzak et al. 2008; Chen et al. 2010a,b; Bordoloi et al. 2011; Nielsen, Churchill & Kacprzak 2013b). The paradigm developed thus far is that the Mg II absorbers are linked with either of the galactic-scale outflows originating from their host galaxies (Bouché et al. 2006; Tremonti, Moustakas & Diamond-Stanic 2007; Martin & Bouché 2009; Weiner et al. 2009; Chelouche & Bowen 2010; Noterdaeme, Srianand & Mohan 2010; Rubin et al. 2010; Lundgren et al. 2012; Bordoloi et al. 2014), dynamical mergers or filamentary accretion on to galaxies (Steidel et al. 2002; Chen et al. 2010a; Kacprzak et al. 2010, 2011, 2012; Martin et al. 2012; Rubin et al. 2012) and high-velocity clouds (Richter 2012; Herenz et al. 2013). Thus Mg II absorbers may be tracing different feedback processes that control the evolution of their host galaxies.

In efforts to determine physical properties of galaxies associated with Mg II absorbers (hereinafter Mg II galaxies), the rest-frame equivalent width (W_{2796}) of Mg II absorption is found to be anticorrelated with impact parameter (ρ), at ∼7.9σ level (Lanzetta & Bowen 1990; Bergeron & Boissé 1991; Steidel 1995; Churchill et al. 2000; Kacprzak et al. 2008; Chen et al. 2010a; Rao et al. 2011; Kacprzak et al. 2013; Nielsen et al. 2013b). This has led to the suggestions that the Mg II absorption could originate from the extended haloes of normal galaxies with unit covering factor for the absorbing gas (see e.g. Petitjean & Bergeron 1990; Srianand & Khare 1994). Recent studies suggest that the scatter in the W_{2796} versus ρ relationship could be further reduced if luminosity-dependent radial extent of the gas is also taken into account (Chen et al. 2010a; Nielsen et al. 2013b). On the contrary, search for Mg II absorption from galaxies close to the QSO line of sight suggested that the gas covering factor is less than unity (Tripp et al. 2005; Barton & Cooke 2009). The Mg II gas distribution may be patchy around galaxies with the gas covering factor decreasing with the increasing impact parameter (Chen et al. 2010a; Nielsen et al. 2013b). While luminous galaxies are frequently identified at the redshift of the Mg II absorption,

★ E-mail: rvjoshirv@gmail.com

question remains that what fraction of these systems are produced by undetected low-luminosity galaxies at much smaller impact parameters (see fig. 10 of Noterdaeme et al. 2010).

The fibre fed spectroscopic observations, e.g. 3- and 2-arcsec diameter fibres employed in Sloan Digital Sky Survey Data Release 7 (SDSS-DR7; Abazajian et al. 2009) and SDSS-DR12 (BOSS; Alam et al. 2015), register photons from all the objects that happen to fall within the fibre along our line of sight. This in principle allows detection of nebular emission associated with the absorbing gas (Wild, Hewett & Pettini 2007; Borthakur et al. 2010; Noterdaeme, Srianand & Mohan 2010; York et al. 2012; Straka et al. 2015). Noterdaeme et al. (2010) have performed an absorption-blind search, that is, without a prior information on absorption, of nebular emission features (e.g. [O II], [O III] and H β) and detected 46 [O III] emitting galaxies at $0 < z < 0.8$ on top of the quasar spectra (hereinafter refer to as GOTOQs), out of which ∼17 are Mg II absorbers at $z \geq 0.4$. The [O III] luminosities of these systems are found to be less than that of an $L^{\star}$ galaxy with a median luminosity of 0.2 $L^{\star}_{[\mathrm{O\,III}]}$ and a typical star formation rate (SFR) in the range of 0.2–20 $\mathrm{M}_{\odot}$ yr^{-1}. Straka et al. (2015) have subsequently increased the number of known GOTOQs to 103 at a median z of 0.15.

A strong correlation is found between the [O II] luminosity surface density ($\Sigma_{[\mathrm{O\,II}]}$) and W_{2796} in the stacked spectra (Noterdaeme et al. 2010; Ménard et al. 2011). This relationship is also found to be evolving with redshift in the sense that a given W_{2796} seems to be associated with larger $\Sigma_{[\mathrm{O\,II}]}$ at high-z compared to that at low-z. Ménard et al. (2011) have suggested that the Mg II absorbers can in principle provide a new probe of the redshift evolution of the SFR density in a luminosity unbiased manner (however, see López & Chen 2012). Increasing the number of direct detections over a large redshift range will allow us to address this more efficiently. With an aim to probe the nature of Mg II absorbers, we have searched for the nebular emission from Mg II absorption systems by utilizing the unprecedented number of these systems found in the SDSS survey (Zhu & Ménard 2013). These direct detections will not only provide the largest sample to study Mg II–galaxy correlation at low-impact parameters over a large redshift range but also help us understand the origin of $L_{[\mathrm{O\,II}]}$ versus W_{2796} correlation seen in the stacked spectra and its redshift dependence so that the utility of Mg II absorbers as a new tracer of star formation in the Universe can be examined.

This paper is organized as follows. Section 2 describes our sample selection criteria and procedure for detecting the nebular emission lines. In Section 3, using the repeat observations of QSOs in SDSS-DR7 and SDSS-DR12, we examine the effect of fibre size on the nebular emission line detections. In Section 4, we present the absorption line properties of systems detected in nebular emission, the detection probability of nebular emission in Mg II systems, and discuss the dependence of [O II] line luminosity on W_{2796} and z. In this section details of observed nebular line ratio and their redshift evolution are also discussed. We also compare the properties derived based on nebular emission with those based on absorption lines. The summary of our study is presented in Section 5. Throughout, we have assumed the flat Universe with $H_0 = 70\,\mathrm{km\ s^{-1}\ Mpc^{-1}}$, $\Omega_{\mathrm{m}} = 0.3$ and $\Omega_{\Lambda} = 0.7$.

2 SAMPLE

In this work, we use the compilation of Mg II systems from the *expanded-version* of JHU-SDSS Metal Absorption Line Catalog[1] (Zhu & Ménard 2013), generated from the SDSS-DR7 and SDSS-DR12. In order to detect the nebular emission line features from the Mg II absorbers, first we have ensured that the most prominent [O II] and [O III] emission lines are covered within the observed wavelength range of SDSS-DR7 (3800–9200 Å) and SDSS-DR12 (3650–10 400 Å) spectra. This criterion limits the redshift range over which [O II] emission can be searched to $0.35 \leq z_{\mathrm{abs}} \leq 0.8$ and $0.32 \leq z_{\mathrm{abs}} \leq 1.0$ for SDSS-DR7 and SDSS-DR12 spectra, respectively. This resulted in our primary sample of 11 000 and 37 000 Mg II absorbers with Mg II equivalent width (W_{2796}) ≥0.1 Å in SDSS-DR7 and DR12 catalogues respectively, where we have searched for the nebular emission lines.

2.1 Search for nebular emission

For the redshift range of interest for this study, the [O II] λλ3727, 3729 emission doublet is the strongest and most suitable nebular line that can be detected over a wide z range in a region free from the most crowded telluric lines (e.g. O I λ5577, O I λ6300 and OH lines). Also [O II] is regarded as a good indicator of the ongoing SFR. For each Mg II absorber, we search for the [O II] λλ3727, 3729 nebular emission lines at the expected location for z_{abs} in the continuum subtracted spectrum. At first, we model the local continuum that includes the continuum light from both the quasar and the galaxy by a low-order (typically a third order) polynomial fit. The significance of the detection of an emission line feature is determined based on the signal-to-noise ratio (SNR; see Hewett et al. 1985; Bolton, Meiksin & White 2004) defined as

$$\mathrm{SNR} = \frac{\sum_i f_i u_i/\sigma_i^2}{\sqrt{\sum_i u_i^2/\sigma_i^2}}, \tag{1}$$

where f_i is the line flux in ith pixel, σ_i is the flux error and u_i is a Gaussian kernel, normalized such that $\Sigma_i u_i = 1$, and its position and width given by the fitted line parameters. Any feature at the expected location of the [O II] line with SNR ≥ 4 is considered as a positive detection in this work.

However, identifications solely based on single emission line (i.e. blended [O II] λλ3727, 3729 lines) alone may lead to a high probability of false positives if the expected wavelength range is affected by (1) poor sky subtraction in the locations of strong sky lines and/or (2) a bad continuum fit around the broad and narrow emission lines of the background quasar. Therefore, to avoid such cases, we have masked the regions around strong sky lines as well as narrow and broad emission lines from QSOs. In addition, any feature with a full width at half-maximum (FWHM) less than the SDSS spectral resolution (∼150 km s^{-1}) are manually checked and then removed if found to be spurious. We detect [O II] emission from 185 Mg II systems in the redshift range $0.35 \leq z_{\mathrm{abs}} \leq 1.1$ at ≥4σ level. Among them, 62 are detected in SDSS-DR7 (with a fibre diameter of 3 arcsec) and remaining 123 are detected in SDSS-DR12 (with a fibre diameter of 2 arcsec) spectra. From these [O II]-detected systems, we also searched for the other emission features such as H βλ4862 and [O III] λλ4959, 5007. Among 62 systems detected in SDSS-DR7, we found 29 systems showing [O III] λ5007 and 13 systems showing H β detected at ≥3σ. In addition, among 123 systems detected in SDSS-DR12, we found 76 systems showing [O III] λ5007 and 46 systems showing H β detected at ≥3σ. The z_{abs} distributions of Mg II systems with the nebular [O II] emission detected in SDSS-DR7 and SDSS-DR12 are shown in Fig. 1.

In the general population of galaxies, a small fraction (i.e. ∼ 8 per cent) shows the [O III] emission being stronger than

[1] http://www.pha.jhu.edu/∼gz323/Site/

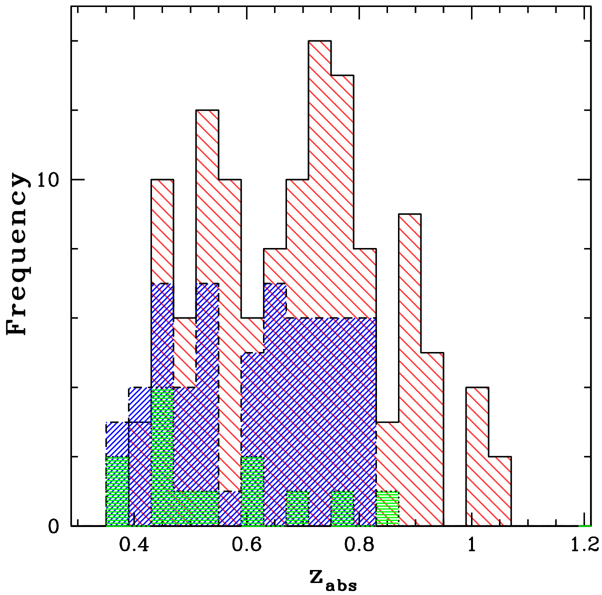

Figure 1. The redshift distribution of Mg II absorbers detected in [O II] emission in SDSS-DR7 (dashed histogram, shaded with slanted lines at 45°) and in SDSS-DR12 (solid histogram, shaded with slanted lines at −45°) spectra. The dotted histogram (shaded with horizontal lines) shows the systems where [O II] and [O III] emission are detected at <4σ and ≥3σ, respectively.

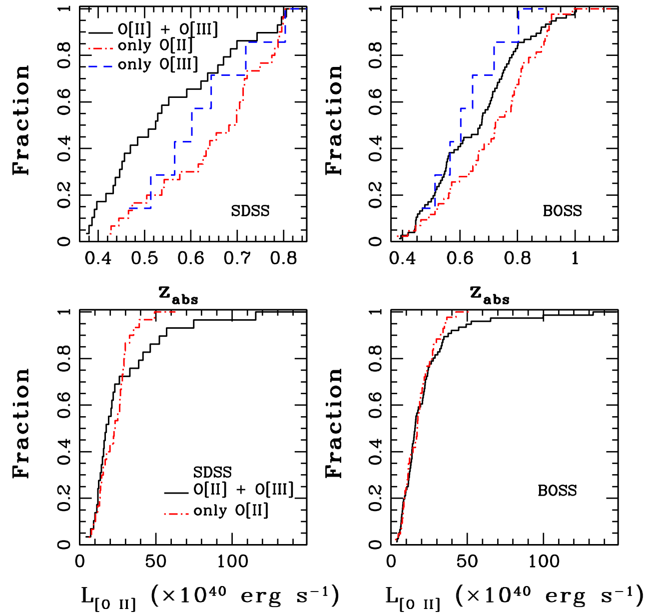

Figure 2. Top panel: cumulative distribution of z_{abs}, for the Mg II absorbers with clear detection of both [O II] and [O III] emission (solid), with only [O II] detection (dot–dashed) and with only [O III] detection (dashed) in SDSS-DR7 (top left) and SDSS-DR12 (top right). Bottom panel: the same for the [O II] luminosity.

[O II]. The nebular line selection based purely on [O II] may miss such systems. In order to account for such systems, we searched for [O III] emission from Mg II absorbers that do not show strong [O II] emission (i.e. at more than 4σ level). We found 13 Mg II systems where [O III] $\lambda\lambda$4959, 5007 emission is clearly detected at ≥3σ level while [O II] $\lambda\lambda$3727, 3729 emission is not detected at the significant level demanded above (i.e. ≥4σ). Thus, in total we have detected nebular emission lines from 198 Mg II absorption systems.

In Fig. 2 (*top panel*), we compare the redshift distribution of the Mg II systems with clear detection of both [O II] and [O III] emission versus the systems with only [O II] detection. This figure (top panels) also shows the z distribution of 13 [O III]-detected systems with weak [O II]. It is clear from the figure that systems with only [O II] detection are preferentially at high redshift. A two-sided Kolmogorov–Smirnov test (KS-test) shows that the two redshift distributions (i.e. with both [O II], [O III] detections and only [O II] detections) are different with a null probabilities of being drawn from same parent distribution p_{null} = 0.03 and 0.04 for the systems detected in SDSS-DR7 and SDSS-DR12, respectively. We find that the [O II] luminosity (total luminosity of two [O II] lines) for these two subsets are similar (see bottom panels of Fig. 2) with KS-test null probability of p_{null} = 0.42, 0.62 for the SDSS-DR7 and SDSS-DR12, respectively. The redshift distribution of [O III]-detected systems are also different, preferentially at low-z. These differences could either mean (i) some observational bias against detecting [O III] emission from high-z galaxies, for example, the poor sky residuals or (ii) a redshift evolution in the [O III]/[O II] ratio. We come back to this in Section 4.6. The details of our sample searched for nebular emission is summarized in Table 1 and the final sample of 198 Mg II systems detected in nebular emission are given in Table 2. The final list of systems with nebular emission is available in the online table. In all cases where we do not have nebular line (i.e. one of [O III], H β or [O II]) detections, we have estimate the 3σ upper limit by assuming the FWHM of the line that is detected.

Table 1. Sample of Mg II absorbers searched for nebular emission.

Catalogue	z	N[a]	[O II] + [O III][b]	[O II][c]	[O III][d]
SDSS-DR7	0.35 ≤ z_{abs} ≤0.8	11523	29	33	6
SDSS-DR12	0.30 ≤ z_{abs} ≤1.1	37038	76	47	7

[a]Total number of Mg II absorbers within the desired z range.[b][O II] is detected at ≥4σ and [O III] is detected at ≥3σ.[c][O II] is detected at ≥4σ and 3σ upper limits on [O III].[d]3σ upper limits on [O II] and [O III] is detected at ≥3σ.

Note that, our compilation of 198 Mg II systems, seen in emission, is the largest sample of Mg II galaxies known till date. Based on previous attempts to study the galaxies associated with Mg II absorbers, only ∼ 182 spectroscopically identified intermediate redshift (0.07 ≤ z ≤ 1.1) galaxies at impact parameters of 5.4 ≤ ρ ≤ 193 kpc are known [see the compilation of Nielsen et al. (2013a, and reference therein)]. In particular, the Mg II systems with nebular emission in our compilation probe very low impact parameters (i.e. ρ ≤ 12 kpc). In the literature, only six galaxies associated with Mg II absorbers are known at such impact parameters. In addition, nebular emission from 17 Mg II systems are identified by Noterdaeme et al. (2010) in the SDSS fibre spectra. Eight of these systems are part of our sample.

2.2 Emission line parameters

We determine the emission line parameters by fitting the [O II] $\lambda\lambda$3727, 3729, H $\beta\lambda$4862 and [O III] $\lambda\lambda$4959, 5007emission lines with Gaussian profiles. We fit all detected lines simultaneously by using a single emission redshift within a velocity offset of ±150 km s^{-1} with respect to the absorption redshift as typically seen in GOTOQs (see Noterdaeme et al. 2010). In the low-resolution SDSS spectrum, the two [O II] $\lambda\lambda$3727, 3729 lines are unresolved. We model the observed [O II] emission with a double Gaussian profile

Table 2. Sample of Mg II absorbers with nebular emission line. The full table is available online.

No	QSO	Plate	MJD	Fibre	z_{qso}	z_{abs}	$L_{[O\,II]}$ ($\times10^{40}$erg s^{-1})	$L_{[O\,III]}$	$L_{H\beta}$	W_{2796} (Å)
1	BOSS-J000910.01 + 110715.6	6113	56219	602	2.6470	0.6804	21.69 ± 1.84	14.78 ± 2.78	10.96 ± 2.11	2.92 ± 0.17
2	BOSS-J004427.51 + 152439.2	6198	56211	086	2.6090	0.7142	22.03 ± 2.31	16.76 ± 2.66	<6.43	2.77 ± 0.61
3	SDSS-J020317.22 − 010122.8	0701	52179	087	1.7210	0.7253	26.10 ± 6.55	<31.89[a]	<32.67	2.10 ± 0.51
4	SDSS-J023618.98 − 000529.1	0408	51821	237	0.9806	0.6448	17.16 ± 4.17	<13.70	<11.58	1.26 ± 0.40
5	SDSS-J030730.61 − 074555.6	0459	51924	309	0.7543	0.6986	28.81 ± 3.33	45.09 ± 8.49	<13.40	2.34 ± 0.27
6	SDSS-J074850.59 + 165625.5	1920	53314	217	0.9321	0.6651	21.86 ± 3.49	<15.02	12.82 ± 4.56	2.07 ± 0.26
7	SDSS-J081121.39 + 451719.4	0439	51877	554	0.8907	0.6702	20.42 ± 3.26	<21.16	<17.61	0.92 ± 0.09
8	SDSS-J084507.04 + 311003.0	1270	52991	266	1.0903	0.6370	35.03 ± 8.22	<12.12	<18.77	0.95 ± 0.12
9	SDSS-J085051.97 + 083026.6	1299	52972	333	0.6635	0.3767	5.56 ± 1.33	2.82 ± 0.88	<2.16	1.75 ± 0.15
10	SDSS-J085846.71 + 531643.2	0449	51900	145	1.1859	0.7886	42.37 ± 6.94	<93.84	<25.97	1.77 ± 0.08

[a] 3σ upper limit.

with a tied linewidth but freely varying the line ratio in a range of 3.4–1.5.[2] This allows for probing the typical range in the electron density of the gas under photoionization equilibrium. The H β and [O III] $\lambda\lambda$4959, 5007 emission lines are modelled with a single Gaussian each. The integrated line intensities of [O II] $\lambda\lambda$3727, 3729, [O III] $\lambda\lambda$4959, 5007 and H β are then measured from the fitted Gaussian parameters.

In Fig. 3, we present few examples of the nebular emission line spectra of Mg II systems in our sample along with the results of our best-fitting Gaussian profiles. The lower three panels show examples of clear detections of [O II], H β and [O III] emission lines. In the upper two panels, we show examples where [O II] is clearly detected whereas the [O III] region is affected by the night sky emission. In addition, third panel from the top shows an example of GOTOQ system where [O III] emission is clearly seen without a clear detection of the [O II] line.

3 FIBRE SIZE EFFECT

Our sample of Mg II systems that show nebular emission lines spans a substantial redshift interval, ranging from 0.4 to 1.1. In this range, the fibre with an aperture of 3 arcsec, used in SDSS-DR7 spectra, corresponds to a projected radius (i.e. an upper limit on the impact parameter) of ∼8.1−12.3 kpc. Similarly, the 2 arcsec fibre used in SDSS-DR12 corresponds to a radius of ∼5.4−8.2 kpc. Before performing different statistical analysis, it is important for us to understand various possible biases introduced by the finite size of fibres used. For this, we used the repeated spectroscopic observations of quasars in SDSS-DR7 and SDSS-DR12. Including the GOTOQs listed in Straka et al. (2015) we have found 39 cases with repeat observations using fibre of two different sizes.

In Fig. 4, we compare the ratio of [O II] luminosities measured between SDSS-DR7 (i.e. $L^{s}_{[O\,II]}$) and SDSS-DR12 (i.e. $L^{b}_{[O\,II]}$) fibre spectra as a function of the absorber redshift. For this comparison, we consider only systems where the nebular emission line is clearly detected at least in one epoch spectrum. As expected the measured luminosities in the SDSS-DR7 spectra are higher than those of SDSS-DR12 spectra in several cases. Contrary to our expectation, 18 per cent of Mg II systems at $z > 0.4$ show slightly larger luminosity in the SDSS-DR12 spectrum albeit within $\sim2\sigma$ level. This is possible when there are issues related to centring of the quasars in the fibre during spectroscopic observations or effect of varied seeing between two epochs. In addition, there could also be issues related to flux scales, where SDSS-DR12 spectra tend to show excess flux in the blue. We consider the scatter in [O II] luminosity ratio as the level at which we cannot quantify the flux difference over the redshift range of our interest (i.e. $0.35 \le z_{abs} \le 1.1$), shown as dotted lines in Fig. 4. It is interesting to note that the fluxes in the SDSS-DR12 and SDSS-DR7 agree within the 1σ uncertainty in most of the cases. It is clear from Fig. 4 that the fibre size effect is severe at low-z. Considering the 1σ uncertainty, the fraction of systems with similar fluxes in SDSS-DR7 and DR12 is found to be 8 per cent, 42 per cent and 50 per cent for the three redshift ranges of $z < 0.35$, $0.35 \le z \le 0.6$ and $z \ge 0.6$ (see top panel of Fig. 4). In Fig. 5, we show three examples demonstrating the fibre size effect where the [O II] luminosity seen in SDSS-DR7 (*thick solid line*) spectrum is found to be larger (*top panel*), smaller (*middle panel*) and similar (*bottom panel*) to those measured in the SDSS-DR12 (*thin solid line*) spectrum.

Next, in Fig. 6 we plot the [O II] luminosity ratio (i.e. $L^{s}_{[O\,II]}/L^{b}_{[O\,II]}$) against the $L_{[O\,II]}$ measured in SDSS-DR7 spectra, i.e. $L^{s}_{[O\,II]}$, and W_{2796}. It is clear from the top panel of Fig. 6 that a large scatter in $L^{s}_{[O\,II]}/L^{b}_{[O\,II]}$ is preferentially present for systems with low $L_{[O\,II]}$. It is quite possible that the line emitting region is partially covered by the fibre that leads to the lower $L_{[O\,II]}$. This figure also demonstrates that the observed [O II] luminosity in the SDSS-DR12 spectra could be underestimated by up to a factor of 3 due to fibre size effects.

Recently, Paulino-Afonso et al. (2017) have found that the effective radius (r_e) of H α-selected galaxies (relevant for the present study) shows a mild decrease over increasing z. They measured a median size of $r_e \sim 4$ kpc at $z \sim 0.4$. If we assume this size for the nebular line emitting regions studied here then at $z \sim 0.4$ all [O II] luminosity from the galaxies within r_e will be observed only when $\rho < 4.1$ and <1.4 kpc in the case of SDSS-DR7 and SDSS-DR12, respectively. Therefore, if we assume ρ of our detections to be uniformly distributed within the fibre then only in ≤25 per cent and ≤7 per cent cases we expect fibre loss to be negligible in the case of SDSS-DR7 and SDSS-DR12 spectra, respectively, at $z \sim 0.4$. However, at $z \sim 0.8$ the median $r_e \sim 3.3$ kpc. In this case, we will detect full [O II] nebular emission in ∼50 per cent cases for SDSS-DR7 and ∼32 per cent cases for SDSS-DR12. The probability of Mg II galaxy in our sample not suffering the fibre loss, measured as

[2] The [O II] $\lambda3729/\lambda3727$ intensity ratio in the range 3.4–1.5 is predicted in photoionization models for the electron density in the range $n_e = 10^1$–10^5 cm^{-3} for the kinetic temperature $T = 10\,000°$ K (Osterbrock & Ferland 2006).

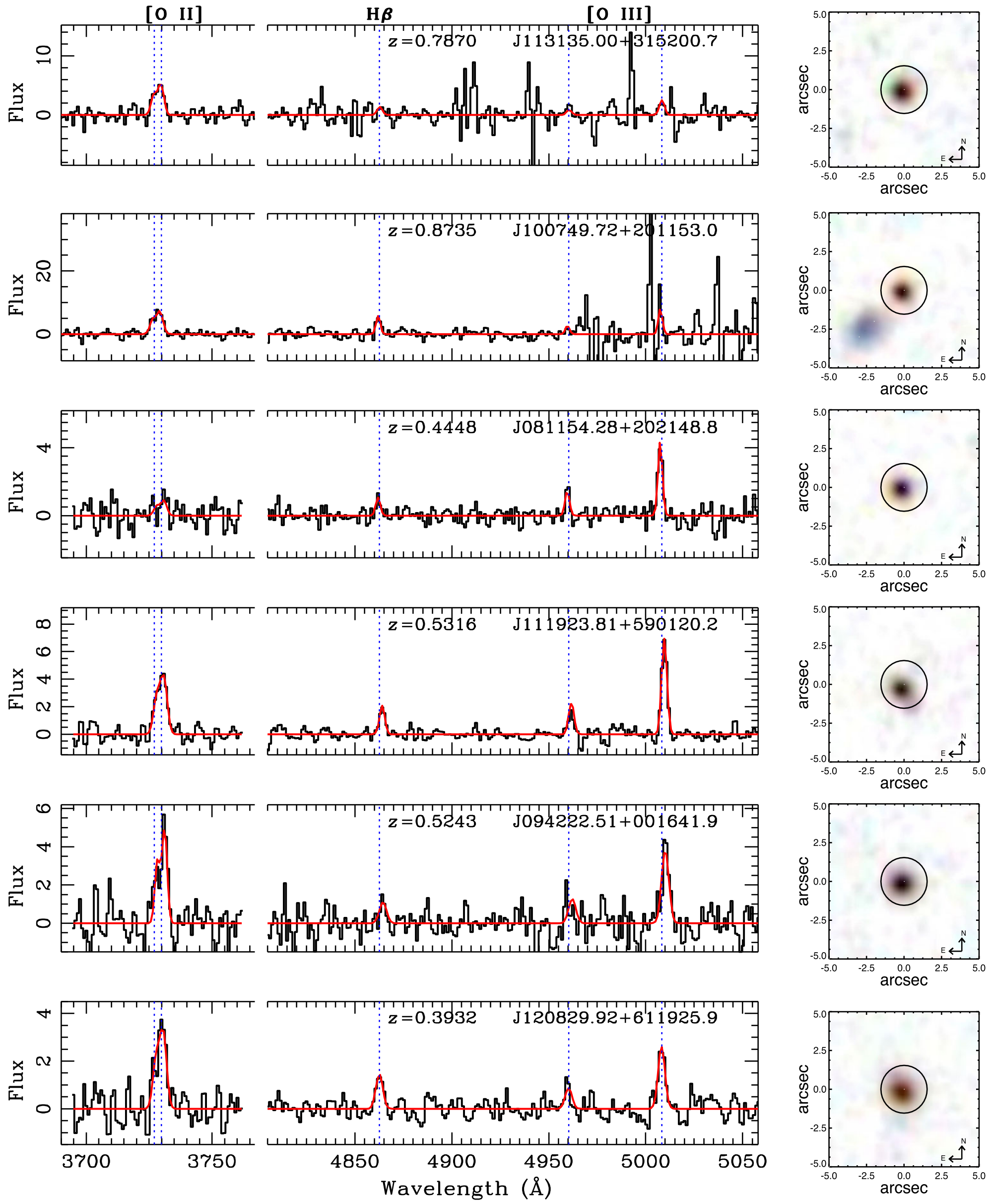

Figure 3. Examples of nebular emission lines detected in the continuum subtracted spectra from the intervening Mg II systems, the flux scale is in units of 10^{-17} erg s^{-1} cm^{-2} Å^{-1}. In each panel, QSO name and absorption redshift are indicated, and vertical dashed lines indicate different nebular emission lines marked at the top panel. In the right-hand panels, we show the image stamp of size ∼10 arcsec around the quasars. The circle represents the position of the 3-arcsec diameter SDSS-DR7 fibre.

$((r_{\rm fibre} - r_{\rm e})/r_{\rm fibre})^2$, as a function of z for SDSS-DR7 (*solid curve*) and SDSS-DR12 (*dotted curve*), are shown in the top panel of Fig. 4. Here, $r_{\rm fibre}$ is the projected radius of the fibre at the redshift of the Mg II systems. We consider this as an upper limit as a detection can occur even when the impact parameter is slightly larger than the fibre (i.e. when $r_{\rm fibre} \geq \rho - r_{\rm e}$). It is clear from the above discussions that our measurements of nebular line luminosities are affected by fibre size effects and this effect has a clear redshift dependence.

4 RESULTS

In what follows we study the emission line properties of Mg II absorbers and compare these with the properties derived using absorption lines.

4.1 Absorption line properties

In order to see the fibre size effect on the absorption line properties, we first compare W_{2796}, Mg II doublet ratio (DR = $W_{\rm Mg\,II\lambda2796}/W_{\rm Mg\,II\lambda2803}$) and $W_{\rm Fe\,II\lambda2600}/W_{\rm Mg\,II\lambda2796}$ (defined as R) of the Mg II absorbers with [O II] detections in SDSS-DR7 and DR12 data set. Naively we would have expected the average W_{2796} to be slightly lower in the case of SDSS-DR7 as it also could have sightlines with slightly larger impact parameters due to larger fibre size. A two-sided KS-test finds no difference between the two subsets based on W_{2796}, DR and R parameters with a null probability of being drawn from same parent distribution of $P_{\rm KS}$ = 0.4, 0.2 and 0.4, respectively. The lack of any significant difference can be attributed to the flattening of W_{2796} versus ρ and possible scatter in this relationship. We come back to this in Section 4.8.

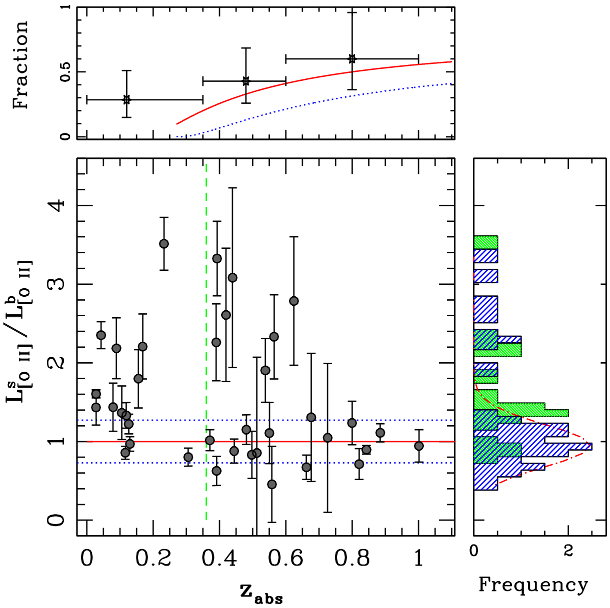

Figure 4. The [O II] luminosity ratio measured between SDSS-DR7 and SDSS-DR12 spectra (i.e. $L^{s}_{[\mathrm{O\,II}]}/L^{b}_{[\mathrm{O\,II}]}$) as a function of absorber redshift. The right-hand panel shows the histogram of $L^{s}_{[\mathrm{O\,II}]}/L^{b}_{[\mathrm{O\,II}]}$ for the systems detected at high (i.e. $z > 0.36$) redshift (solid histogram, shaded with slanted lines at 45°) and fitted with Gaussian function and at low (i.e. $z < 0.36$) redshift (dashed histogram, shaded with slanted lines at −45°). The top panel shows the fraction of systems with $L_{[\mathrm{O\,II}]}$ consistent within 1σ range over three redshift bins. The solid (respectively, dotted) curve represents the expected z dependence of absorber galaxy being inside the SDSS-DR7 (respectively, SDSS-DR12) fibre (see Section 3 for details).

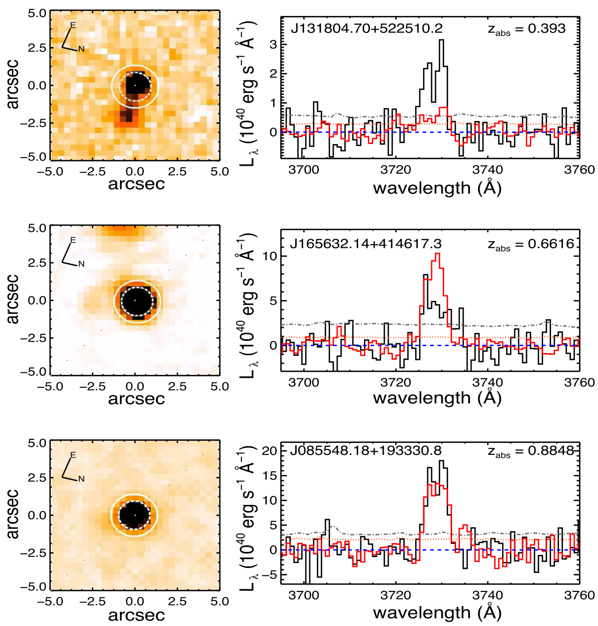

Figure 5. Right-hand panels: examples of variation in [O II] nebular emission line luminosity with change in fibre size from 3 to 2 arcsec in SDSS-DR7 (thick solid line) and DR12 (thin solid line) spectrum, respectively. The error spectra of SDSS-DR7 and SDSS-DR12 are shown as dot–dashed and dotted lines. Left-hand panels: image stamp of size ∼ 10 arcsec around the quasar. The dotted and solid circles represent the size corresponding to 2- and 3-arcsec diameter of SDSS-DR12 and SDSSS-DR7 fibre spectra, respectively. Note that, the fibre centring may be slightly different than what is shown here.

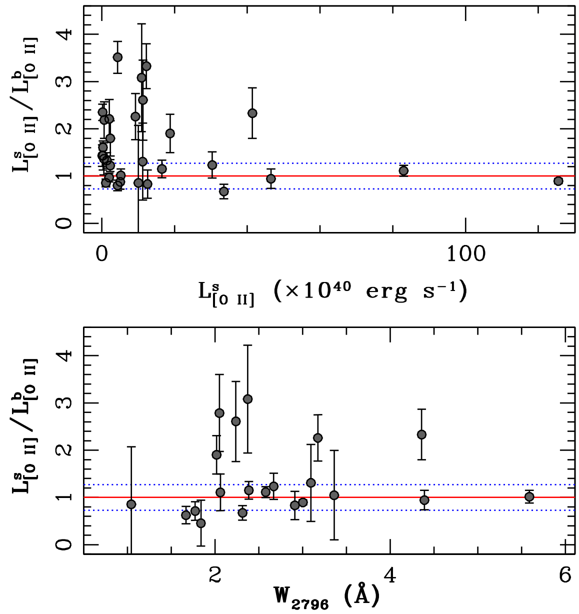

Figure 6. Top panel: the [O II] luminosity ratio measured in SDSS-DR7 and DR12 spectra as a function of [O II] luminosity detected in SDSS-DR7 spectra. Bottom panel: the [O II] luminosity ratio as a function of W_{2796}.

Next, we compare the distribution of DR and R of the Mg II systems with and without detection of the nebular emission lines. At first, we found that all but eight Mg II systems detected in emission (both in DR7 and DR12) have $W_{2796} \geq 1$ Å, with mean W_{2796} of ∼ 2.3 and 2.4 Å for the SDSS-DR7 and SDSS-DR12, respectively. In Fig. 7 (*lower panel*), we show the distribution of W_{2796} from the Mg II systems with detected nebular emission line with the overall Mg II absorbers in our primary sample. It is clear from the figure that Mg II systems with nebular emission are predominantly distributed towards higher W_{2796}.

Using deep imaging of seven Mg II systems with [O II] nebular emission at $z \sim 0.1$ with $\rho < 6$ kpc, Kacprzak et al. (2013) have argued that these systems are consistent with W_{2796} distribution of the Milky Way (MW) interstellar medium (ISM) and ISM+Halo. Following their approach, in the *top panel* of Fig. 7, we compare the W_{2796} distribution of systems with nebular emission in our sample with those measured from different components of MW. For this, we use 71 Mg II absorption lines produced by MW (ISM+halo gas) and 21 systems as halo gas identified along the sightlines of 83 quasars, observed in Hubble Space Telescope Quasar Absorption Line Key Project (Bahcall et al. 1993), by Savage et al. (2000). The W_{2796} distribution for the Mg II systems with [O II] emission, MW(ISM+halo) and MW(halo gas) is shown in the *upper panel* of Fig. 7. In view of the fact that MW sightlines pass halfway through the disc/halo, we have applied a correction factor of two in the W_{2796} for MW systems (Kacprzak et al. 2013). This figure clearly indicates that for a large fraction of Mg II systems with [O II] emission, the Mg II absorption tends to be strong and their distribution is closer to what has been seen for MW (ISM+halo). A simple two-parameter KS-test confirms this.

Using a photoionization modelling, Srianand (1996) has shown that the Mg II absorbers with $R \geq 0.5$ trace systems with high N(H I), preferentially the damped Ly α absorbers (DLAs; see also Rao, Turnshek & Nestor 2006; Gupta et al. 2012; Dutta et al. 2017). Furthermore, Rao et al. (2006) have shown that the fraction of Mg II systems that are DLAs increases with the W_{2796}. In order to find

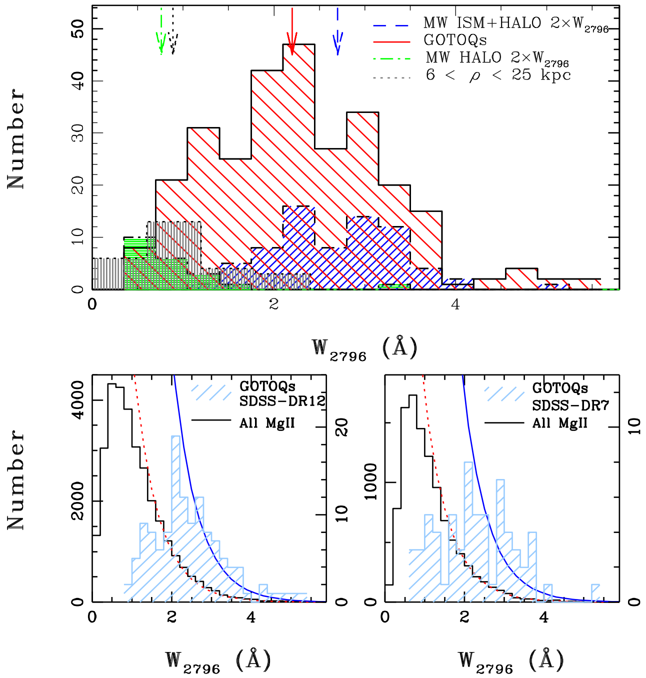

Figure 7. Upper panel: a comparison of the Mg II equivalent width (W_{2796}) distribution of GOTOQs (solid histogram) with the Mg II systems having $6 < \rho < 25$ kpc (dotted histogram, shaded with vertical lines) and those through the Milky Way [MW] ISM+halo (dashed histogram, shaded with slanted lines at 45°) and MW halo (dot–dashed histogram, shaded with horizontal lines). For the MW systems, a correction factor of 2 is applied as sightlines are intercepted halfway through the disc/halo. The median W_{2796} for each sample is marked as an arrow on top. Lower-left panel: distribution of Mg II rest equivalent widths for the overall SDSS-DR12 Mg II sample (with $z_{\rm abs}$= 0.3–1.1, unfilled histogram) and the Mg II absorbers that show nebular emission (hatched histogram). The two distributions are represented with different scales for presentation purpose only (SDSS in the left, galaxy sample in the right-hand side ordinates). The dotted and solid curves represent the parametrization by Zhu & Ménard (2013), scaled to match the number of systems with $W_{2796}\geq 2$ Å. Lower-right panel: same as left for the SDSS-DR7 Mg II absorbers.

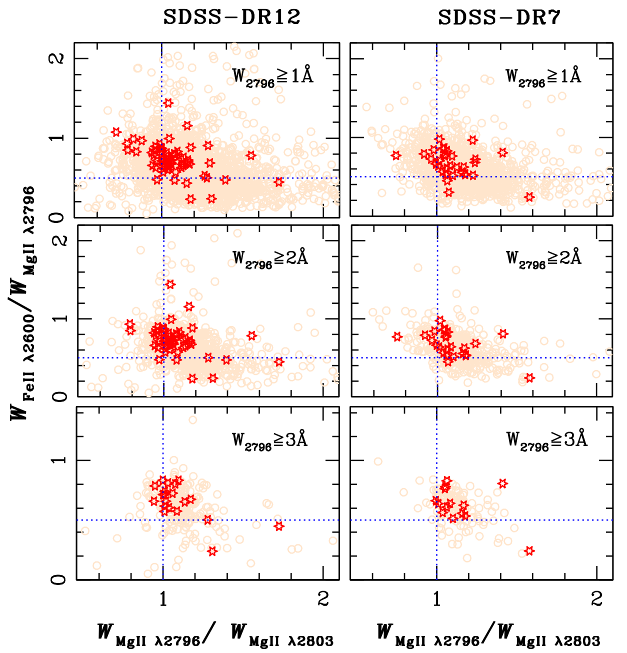

Figure 8. The Mg II DR versus R parameter of Mg II absorbers with and without nebular emission line detection for $W_{2796}\geq 1$ Å (top), ≥ 2 Å (middle) and ≥ 3 Å(bottom) in the SDSS-DR12 (left-hand panel) and SDSS-DR7 (right-hand panel) samples. Open circles are for the full sample and red stars are for Mg II systems with nebular emission.

if the Mg II absorbers that show nebular line emission occupy any preferred location in the parameter space defined by the equivalent width ratios of metal absorption, we plot the DR versus R in Fig. 8, for systems with and without nebular emission detection over various W_{2796} bins (i.e. $\geq$ 1, 2 and 3 Å). It is clear from the figure that among the strong Mg II absorbers, the systems showing nebular emission are preferentially having a small DR, close to unity, and the R parameter greater than 0.5, plotted as *dotted* horizontal line. These differences were also confirmed when we do the KS statistics.

Interestingly, Rao et al. (2006) have shown that the success rate of identifying DLAs can be enhanced if one puts additional constraints based on other metal lines, e.g. $R >$ 0.5 and W(Mg I) >0.1 Å. In recent efforts to detect cold gas in strong Mg II systems, by using H I 21-cm absorption, it has been found that the detection rate of H I 21-cm absorption is about four times higher in systems with strong Fe II at $0.5 < z < 1.5$ (see Gupta et al. 2012; Dutta et al. 2017). For the average W_{2796} (i.e. ∼2 Å) seen in our sample, the probability of Mg II system being DLA is found to be ∼50 per cent (Rao et al. 2017, see their fig. 2). In addition, the N(H I) versus W_{2796} relation by Ménard & Chelouche (2009) shows that the GOTOQs belong to the sub-DLA systems with log N(H I) of ∼20.1, albeit having a large scatter in N(H I) up to about 3 orders of magnitude. Therefore, a good fraction of our systems will be DLAs.

4.2 Detection probability of nebular emission lines in strong Mg II systems

The detection of the nebular emission from the Mg II systems not only depends on the emission line flux but also on (i) the flux of the background quasar, (ii) the dust attenuation of emission lines in the host galaxy and (iii) the bias due to fibre size effects, as discussed above. Here, we compute the fraction of [O II] nebular emission line detections as a function of W_{2796} in the SDSS fibre spectra centred around distant quasar that are detected above the luminosity threshold of 0.3, 0.5 and 0.7 $L^{\star}_{\rm [O\,II]}$. For this, we restrict ourselves to a common redshift range of $0.36 \leq z \leq 0.8$ in SDSS-DR7 and DR12 and consider the log $L^{\star}_{\rm [O\,II]}$ (erg s^{-1}) = 41.6 at the average redshift of $z = 0.6$ (Comparat et al. 2016). First, we find the number of sightlines suitable for detecting the [O II] line with a given luminosity threshold at $\geq 4\sigma$ level by integrating the error spectra across the expected location of [O II] doublet, typically comprises of ∼ 12 pixels. Further, the fraction of systems is computed as a ratio between the number of Mg II systems with [O II] emission above a given luminosity threshold to the total number of Mg II systems for which such a line is detectable.

In Fig. 9, we show the detection probability of [O II] emission line as a function of W_{2796} for the luminosity threshold of 0.3 (*top panel*), 0.5 (*middle panel*) and 0.7 times (*bottom panel*) $L^{\star}_{\rm [O\,II]}$. It is apparent from the figure that the detection probability of nebular emission lines increases with the strength of the W_{2796}. The fraction of Mg II systems detected in emission for various luminosity thresholds (in column 1) are listed in the columns 2 and 3 of Table 3. It is also clear from the table that the fractional detection of [O II] in Mg II systems is higher for the low-luminosity threshold. Last column

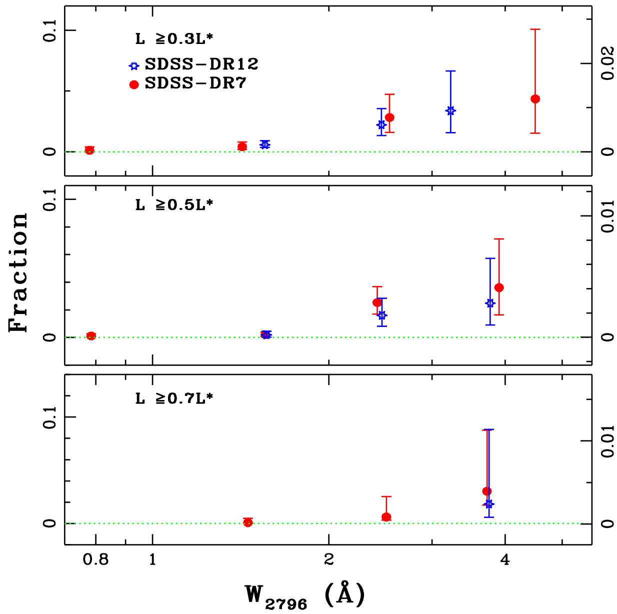

Figure 9. Plot showing the fraction of Mg II systems detected in emission, with a luminosity threshold of $\geq 0.3\ L^{\star}_{[\rm O\,II]}$(top panel), $\geq 0.5\ L^{\star}_{[\rm O\,II]}$(middle panel) and $\geq 0.7\ L^{\star}_{[\rm O\,II]}$(bottom panel) detected in SDSS-DR7 (circle) and SDSS-DR12 (stars) fibre spectra. The fraction for Mg II absorbers in SDSS-DR12 fibre spectra is given in the right-hand side ordinates.

Table 3. Detected fraction of Mg II absorbers, with $W_{2796} \geq 2$ Å, for various luminosity thresholds.

Criteria	SDSS-DR7	SDSS-DR12	Expected fraction
$\geq 0.3\ L^{\star}_{[\rm O\,II]}$	$0.031^{+0.017}_{-0.012}$	$0.007^{+0.003}_{-0.002}$	$0.014^{+0.008}_{-0.005}$
$\geq 0.5\ L^{\star}_{[\rm O\,II]}$	$0.027^{+0.010}_{-0.007}$	$0.002^{+0.001}_{-0.001}$	$0.012^{+0.002}_{-0.003}$
$\geq 0.7\ L^{\star}_{[\rm O\,II]}$	$0.011^{+0.017}_{-0.004}$	$0.001^{+0.003}_{-0.001}$	$0.005^{+0.008}_{-0.002}$

Note. Here, we use $L^{\star} = 4.16 \times 10^{41}$ erg s^{-1}.

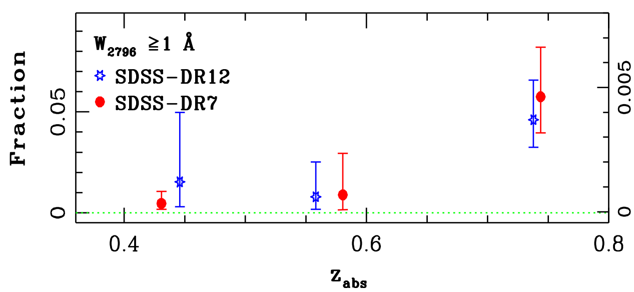

Figure 10. Plot showing the fraction of strong Mg II systems ($W_{2796} \geq 1$ Å) detected in emission, with a luminosity threshold of $\geq 0.3\ L^{\star}_{[\rm O\,II]}$ detected in SDSS-DR7 (circle) and SDSS-DR12 (stars) fibre spectra, as a function of z. The fraction for Mg II absorbers in SDSS-DR12 fibre spectra is given in the right-hand side ordinates.

in Table 3 gives the expected detection rate in the case of SDSS-DR12 if one scales the detection rate in SDSS-DR7 by the ratio of projected fibre areas. This is much higher than the actual rate we find for SDSS-DR12. The difference can be reduced if we consider the nebular line emitting regions to be extended and the fibre size does affects the observed luminosity as we discussed in Section 3.

Furthermore, in Fig. 10 we show the detection probability of nebular emission from strong ($W_{2796} \geq 1$ Å) Mg II systems as a function

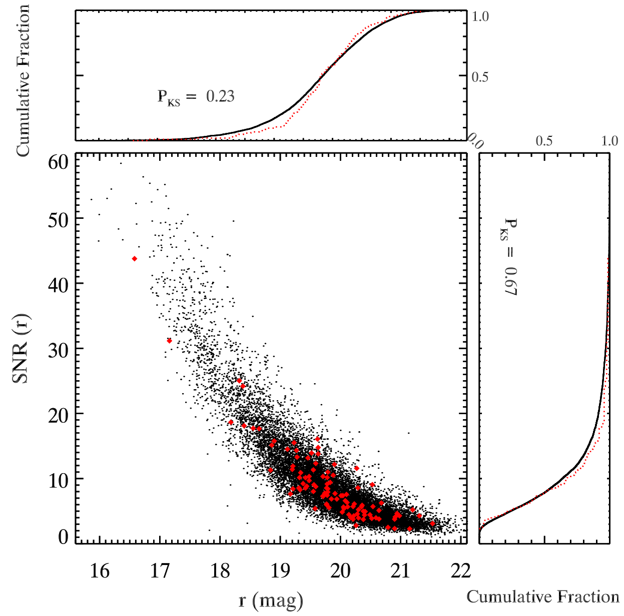

Figure 11. r-band SNR versus magnitudes for quasars with strong ($W_{2796} > 1$ Å) intervening Mg II systems (black dots) and systems detected in [O II] nebular emission lines (red diamond) from SDSS-DR12. The top and right-hand panels show the cumulative distributions of magnitudes and SNR, respectively.

of redshift for a luminosity threshold of 0.3 $L^{\star}_{[\rm O\,II]}$. A rise in the detection probability of nebular emission as a function of redshift is clearly seen. This is expected from the increasing projected area of fibre with z which leads to high probability for the line emitting regions to come inside the fibre. Interestingly, in an effort to model the effect of finite fibre size, López & Chen (2012) have shown that the fraction of systems for which the absorbing galaxy will give rise to [O II] emission in QSO spectra increases as a function of W_{2796} and will depend on the fibre size. They showed that the detection fraction increases from ∼50 per cent for $W_{2796} > 1$ Å to ∼90 per cent for $W_{2796} > 3$ Å when no limiting flux condition is applied. This is what one expects based on the known W_{2796} versus ρ anticorrelation. While what we observe is consistent with the trend presented by López & Chen (2012), the actual detection fraction we find is much less than their model prediction because of the high-luminosity threshold (i.e. 0.3 $L^{\star}_{[\rm O\,II]}$) imposed in our study. Here, we also find that, for a given luminosity threshold, the [O II] detection rate in Mg II systems is higher in the SDSS-DR7 spectra than in the SDSS-DR12 spectra (see Fig. 9).

In Fig. 11, we compare the median SNR measured over all pixels in the r-band to the QSO r-band magnitude for all the QSO spectra from SDSS-DR12 searched here for the nebular emission and hosting an Mg II system with $W_{2796} \geq 1$ Å. A KS-test does not show any statistical difference between the r-band magnitude distributions of the two populations with $P_{\rm KS} = 0.23$. In addition, no difference is seen between the SNR of the two population with $P_{\rm KS} = 0.67$. Thus, it appears that the quasar brightness does not impact the detectability of [O II] nebular emission for systems with $W_{2796} > 1$ Å (see also Noterdaeme et al. 2010).

4.3 The [O II] λλ3727, 3729 luminosity

Results presented in the last two sections suggest, (i) our measured [O II] nebular line luminosity is an underestimation of true

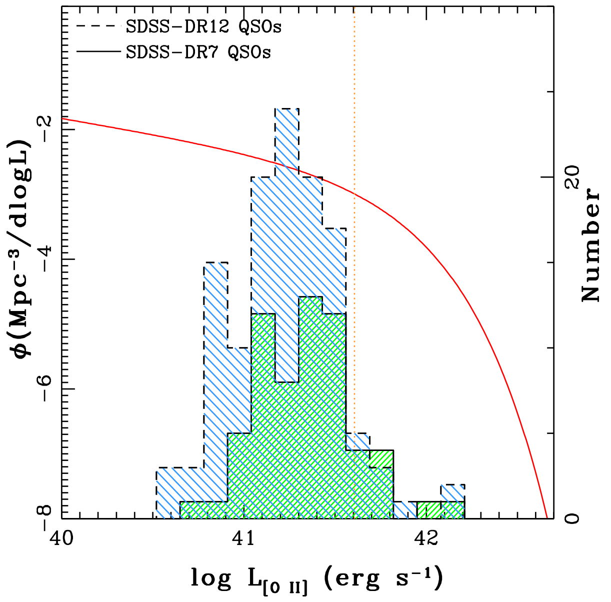

Figure 12. The distribution of [O II] luminosities (lower limit to be precise) for the Mg II absorbers in our sample is compared to the field galaxy [O II] luminosity functions at $z = 0.65$ (solid curve). The vertical dotted line marks the position of $L^{\star}_{[\mathrm{O\,II}]} = 4.1 \times 10^{41}$ erg s^{-1} (Comparat et al. 2016).

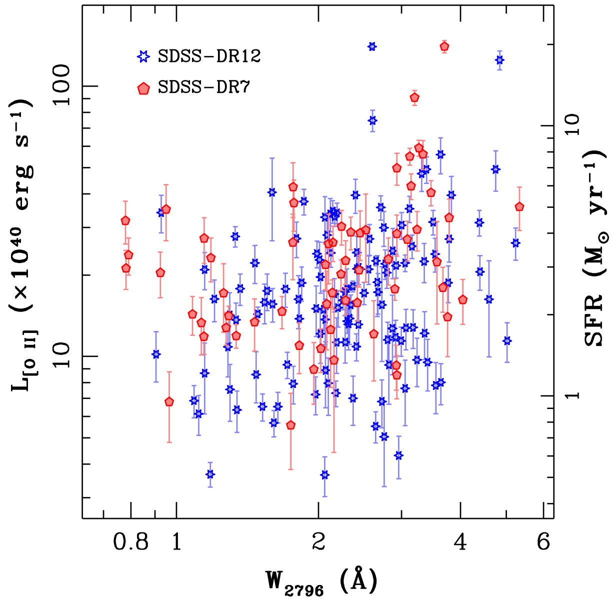

Figure 13. Plot of [O II] luminosity ($L_{[\mathrm{O\,II}]}$) versus W_{2796} for the Mg II systems detected the SDSS-DR7 (pentagon) and SDSS-DR12 (stars). The corresponding SFR is shown in the right-hand side ordinate.

luminosity, (ii) this bias depends on redshift and (iii) the probability of [O II] detection in Mg II systems increases with W_{2796} and z. Keeping these in mind in what follows we study different properties of our Mg II systems with [O II] nebular emission.

In Fig. 12, we compare the distribution of measured [O II] luminosity of Mg II absorbers detected in SDSS-DR7 and SDSS-DR12 spectra with the [O II] luminosity functions of galaxies at $z = 0.65$ from Comparat et al. (2016). Note that, our measured luminosities could very well be lower limits as we do not apply any correction for the dust reddening and the emission line fluxes are affected by fibre losses. Our measured [O II] nebular line luminosities are in the range of 0.14–3.5 $L^{\star}_{[\mathrm{O\,II}]}$ and 0.09–3.5 $L^{\star}_{[\mathrm{O\,II}]}$ in case of SDSS-DR7 and SDSS-DR12, respectively. Therefore, the total luminosity of these Mg II absorbers is typically higher than 0.1 $L^{\star}_{[\mathrm{O\,II}]}$.

Based on the [O II] luminosity, we derive the SFR using prescription given by Kennicutt (1998)

$$\mathrm{SFR}_{[\mathrm{O\,II}]} = (1.4 \pm 0.4) \times 10^{-41} L_{[\mathrm{O\,II}]}. \quad (2)$$

In Fig. 13, we plot $L_{[\mathrm{O\,II}]}$ versus W_{2796} and show the SFR for individual absorbers in the left-hand side ordinate. Bouché et al. (2007) found that 67 per cent of galaxies associated with the Mg II absorbers with W_{2796}>2 Å have SFR in the range 1–20 M$_{\odot}$yr^{-1} at $z \sim 2$ based on the Hα emission having impact parameter in the range 2–54 kpc. We note that about 64 per cent Mg II systems in our sample have W_{2796} >2 Å and SFR > 1 M$_{\odot}$yr^{-1}. This percentage should be considered as a lower limit as our flux measurements are affected by fibre size effects discussed above.

4.4 $L_{[\mathrm{O\,II}]}$ versus W_{2796} correlation?

In this section, using our direct detections, we investigate the origin of the strong correlation seen between W_{2796} and associated [O II] luminosity seen in the stacking analysis of Mg II absorbers (Noterdaeme et al. 2010; Ménard et al. 2011). It is important to note that the same fibre size bias affects both these measurements. In Fig. 13, first we compare the $L_{[\mathrm{O\,II}]}$ as a function of W_{2796} from our direct detections. It is clearly visible that for a given W_{2796} the $L_{[\mathrm{O\,II}]}$ has a wide spread. We have performed the Spearman rank correlation test between $L_{[\mathrm{O\,II}]}$ and W_{2796} and found the correlation coefficient for the Mg II absorbers in SDSS-DR7 fibre spectrum to be r_s(SDSS−DR7) = 0.37 with probability of null correlation $p_{\rm null}$(SDSS−DR7) = 0.003 (a correlation significant at $\sim 3\sigma$). We find similar results for our SDSS-DR12 sample also. Therefore, only a moderately significant correlation is present between $L_{[\mathrm{O\,II}]}$ and W_{2796} when we consider individual detections. In addition, lack of correlation is confirmed using survival analysis when we include all the Mg II absorbers from our sample with [O II] non-detections as upper limits.

Note that in Noterdaeme et al. (2010) and Ménard et al. (2011) a correlation is found between luminosity per unit area ($\Sigma_{[\mathrm{O\,II}]}$) and W_{2796}. It was argued that the fibre effects can be taken care of by normalizing the observed line luminosity by the projected area of the fibre. To compare with this finding, in Fig. 14 we show the dependence of surface brightness of [O II] emission (denoted by $\Sigma_{[\mathrm{O\,II}]}$) as a function of W_{2796}. For plots in the left-hand panel, we assume the surface area to be that of the fibre and for the plot in the right-hand panel, we assume area to be the average effective area of the galaxies at the corresponding absorber redshift. In this figure, we also show the relationship found by Ménard et al. (2011). The surface star formation rate ($\Sigma_{\rm sfr}$) derived from $\Sigma_{[\mathrm{O\,II}]}$ are also indicated in the right-hand side ordinates of both the panels. It is clear that our direct detections do not follow the trend seen in the stacked spectra. A simple correlation analysis suggests that the correlation could at best be at the level of $\sim 2\sigma$. A similar dependence is seen when we compare the W_{2796} with $\Sigma_{[\mathrm{O\,II}]}$, obtained by considering the area of the galaxies at the corresponding absorber redshift. As discussed in Section 3, the observed luminosity can be affected by the fibre size effects that are also redshift dependent.

To see if the above found mild correlation is driven by W_{2796} or not, we divide the sample into three redshift bins of $0.35 \le z < 0.5$ and $0.5 \le z < 0.7$, and $z \ge 0.7$. It is clear from the figure

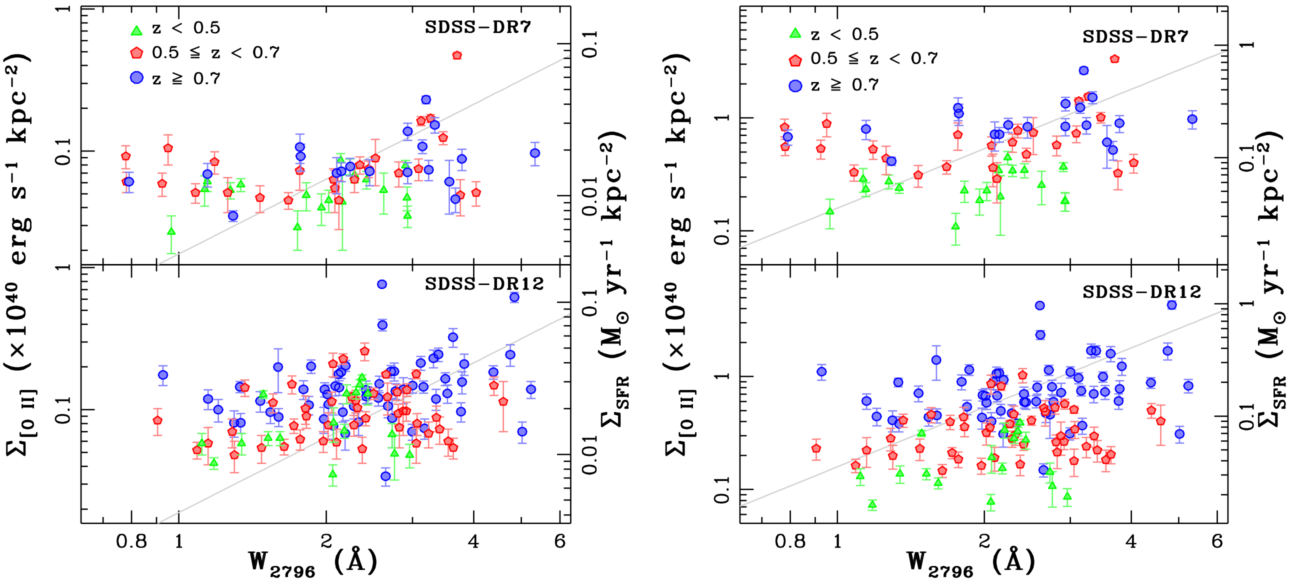

Figure 14. Left-hand panel: the [O II] luminosities surface density ($\Sigma_{[O\,II]}$), while considering the surface area equal to the fibre, as a function of W_{2796} for the Mg II systems detected in the SDSS-DR7 (top panel) and SDSS-DR12 (bottom panel), respectively. The solid grey line shows the best-fitting relation between $\Sigma_{[O\,II]}$and W_{2796} obtained from the stacking analysis by Ménard et al. (2011). The right-hand side axis shows the surface SFR corresponding to $\Sigma_{[O\,II]}$. Right-hand panel: the same for the $\Sigma_{[O\,II]}$ obtained by considering the area of a typical galaxy at the absorber redshift.

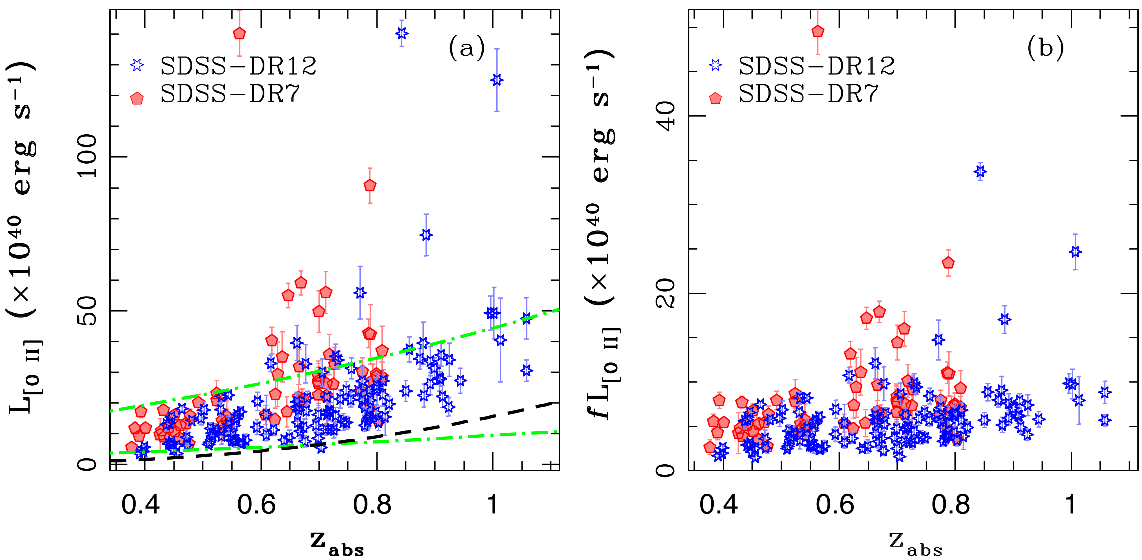

Figure 15. Panel (a): the [O II] luminosity ($L_{[O\,II]}$) of Mg II absorbers with nebular emission as a function of redshift within 3 arcsec fibre (pentagon) in the SDSS-DR7 and within 2 arcsec fibre (stars) in SDSS-DR12 spectra. The lower dot–dashed line shows the expected [O II] luminosity from a 0.15 $L^{\star}_{[O\,II]}$ galaxy as a function of redshift. This provides a lower envelop to the observed data. The upper dot–dashed line shows the expected [O II] luminosity from a 0.7 $L^{\star}_{[O\,II]}$ galaxy as a function of redshift. Panel (b): the scaled $L_{[O\,II]}$, after correcting for the evolution of $L^{\star}_{[O\,II]}$ with z, where $f = L^{\star}_{[O\,II]}(z=0)/L^{\star}_{[O\,II]}(z)$.

that for a given W_{2796}, systems at high redshift show the higher $\Sigma_{[O\,II]}$. However, no clear trend is evident in the individual redshift bins between $\Sigma_{[O\,II]}$ and W_{2796} in both SDSS-DR7 and SDSS-DR12 samples.

In summary, we conclude that among direct detections there is no statistically significant correlation between W_{2796} and $L_{[O\,II]}$ when we restrict ourselves to small redshift intervals. This conclusion is valid for the $\Sigma_{[O\,II]}$ calculated under both the assumptions mentioned above. From the discussion presented in Section 4.2, we find that the fraction of Mg II absorber showing such nebular emission increases with increasing W_{2796}. Therefore, more systems with weaker or no nebular emission have contributed to the stacking at low W_{2796} compare to those at higher W_{2796}. This could explain the strong correlation found between $L_{[O\,II]}$ and W_{2796} in the stacked spectra.

4.5 $L_{[O\,II]}$ versus z

We now explore the redshift dependence of $L_{[O\,II]}$ associated with our Mg II absorbers. In panel (a) of Fig. 15, we see a clear increasing trend of $L_{[O\,II]}$ with z_{abs}. The Spearman rank correlation test finds a strong correlation, with $r_s(\mathrm{SDSS{-}DR7}) = 0.72$ and $r_s(\mathrm{SDSS{-}DR12}) = 0.74$ between $L_{[O\,II]}$ and z_{abs} with a null probability of $p_{null} = 10^{-11}$ (significant at 5.7σ) and $\sim 10^{-22}$ (significant at 8.1σ), respectively. This could be a real redshift evolution of the

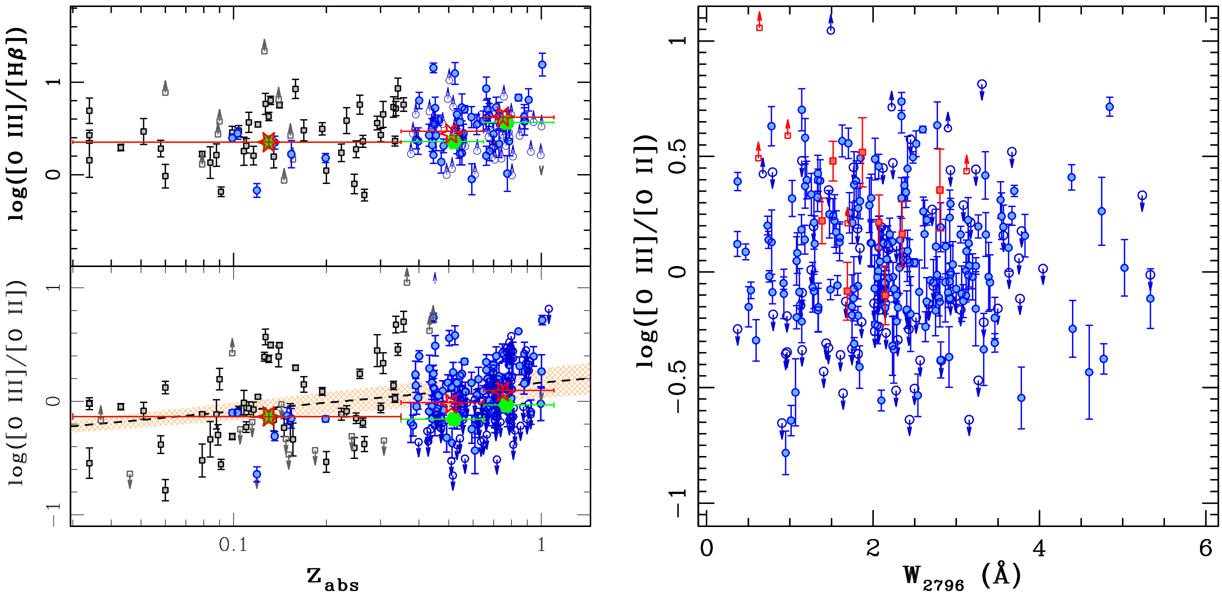

Figure 16. Left-hand panel: the [O III]/H β (top) and [O III]/[O II] (bottom) line ratios as a function of z. The Mg II systems detected in nebular emission line in our sample are shown in circles, while the systems detected by Straka et al. (2015) are shown in squares. The measured [O III]/[O II] ratio in the stacked spectra over three redshift bins is shown in hexagon. The ratio while considering only the systems with [O III] detected at $\geq 3\sigma$ is shown as filled circles/squares. The upward(downward) arrows represent the 3σ upper (lower) limits. The redshift evolution of [O III]/[O II], best described by a power-law fit by Khostovan et al. (2016) is shown as dashed line along with a 1σ uncertainty (shaded region). Right-hand panel: the [O III]/[O II] ratio as a function of W_{2796}. The squares represent the systems with strong [O III] emission.

[O II] luminosity; or some observational artefact due to (i) luminosity bias for a given flux threshold as a function of z (as discussed in Section 3); (ii) the constant fibre size corresponding to more projected area at high z. We explore these one by one.

In panel (a) of Fig. 15, the dashed line shows the expected luminosity for the observed flux of 10^{-17} erg s^{-1} cm^{-2}, corresponding to the minimum luminosity seen in our sample at $z = 0.4$. This line provides a nice lower envelope to the observed luminosity at $z < 0.7$. In the same panel, the *dot–dashed* lines show the expected luminosity of 0.15 and 0.7 $L^{\star}_{[\mathrm{O\,II}]}$ as a function of z using the redshift evolution of field galaxies luminosity function of Comparat et al. (2016, see their table 7). While this luminosity range encompasses the observe luminosity at $z < 0.6$ (barring one system), at high z there are much more galaxies brighter than the 0.7 $L^{\star}_{[\mathrm{O\,II}]}$ galaxies. As discussed in Section 3, lower the redshift higher will be reduction in the measured luminosity compared to the actual luminosity due to fibre effects. Thus, the dominant factor for this $L_{[\mathrm{O\,II}]}$–z relationship explored in the plots could be the redshift dependence of the fibre losses. In addition, the lack of low-luminosity detections at high-z is probably biased due to the observing strategy in SDSS-DR12 where to maximize the flux in the blue part an offset was applied to the position of the quasar target fibres to compensate for atmospheric refraction (see also Pâris et al. 2012).

We can account for the relative increase in characteristic luminosity of galaxies as a function of z by scaling down the observed $L_{[\mathrm{O\,II}]}$ by a factor $f = L^{\star}_{[\mathrm{O\,II}]}(z=0)/L^{\star}_{[\mathrm{O\,II}]}(z)$ (Comparat et al. 2016). The scaled luminosity is shown in panel (b) of Fig. 15. The Spearman rank correlation test finds a correlation with $r_s(\mathrm{SDSS-DR7}) = 0.48$ and $r_s(\mathrm{SDSS-DR12}) = 0.45$ between $L_{[\mathrm{O\,II}]}$ and z_{abs} with a null probability of $p_{\mathrm{null}} = 10^{-3}$ (significant at 3.6σ) and $\sim 10^{-8}$ (significant at 5.3σ), respectively. This indicates that the above correlation is not dominated mainly by the redshift evolution of luminosity. This once again confirms that the fibre size effect is a dominant effect.

In summary, as shown by the field galaxies, [O II] luminosity of our Mg II absorbers are higher at higher z. The correlation remains even after we account for redshift evolution of $L_{[\mathrm{O\,II}]}$. Therefore, we conclude that the strong correlation seen between $L_{[\mathrm{O\,II}]}$ and z in our sample (as well as stacked spectra in the literature) is influenced substantially by the redshift-dependent fibre losses.

4.6 [O III]/[O II] and [O III]/H β nebular line ratio

The [O III]/[O II] and [O III]/H β ratios are sensitive to the hardness of the ionizing radiation field, and serves as a ionization parameter diagnostic of a galaxy (Baldwin, Phillips & Terlevich 1981; Kewley et al. 2001). A rise in ratios of nebular emission lines, in particular [O III]/[O II] and [O III]/H β, of star-forming galaxies is seen over the redshift range $z = 0$–5 (see Nakajima & Ouchi 2014; Steidel et al. 2014; Kewley et al. 2015; Khostovan et al. 2016). This implies that typical galaxies at high redshifts have higher ionization parameter, lower metallicity, harder stellar ionizing radiation field and higher electron densities compare to those of local galaxies. The direct detection of nebular emission lines from Mg II absorbers allows us to explore their physical conditions. We assume that the nebular line ratios do not depend on the fibre size used in the SDSS-DR7 and SDSS-DR12 spectra. Therefore, while studying the emission line ratios we have combined the SDSS-DR7 and SDSS-DR12 samples of Mg II absorbers with nebular emission.

First, we explore the dependence of [O III]/[O II] and [O III]/H β nebular line ratios with redshift (see Fig. 16). While computing the line ratios for cases where the [O III] or H β line is not detected, we use the 3σ upper limits. In addition, we have excluded systems for which both the lines are not detected. In Fig. 16, the limits are shown as (*arrows*) and the detections ($\geq 3\sigma$) are shown with *circles*. For a subset of galaxies with firm detections, we detect a significant correlation between the [O III]/[O II] line ratio with z, with a Kendall's rank correlation coefficient (r_k) of 0.3 with null probability $p_{\mathrm{null}} = 0.006$

Table 4. Redshift evolution of line ratios, metallicity and ionization parameter of Mg II absorbers.

Redshift (z)	Systems	log ([O III]/[O II])	log ([O III]/H β)	log (Z)	log (q)
$0.10 \le z < 0.35$	79	-0.13 ± 0.03	0.35 ± 0.04	$8.33^{+0.19}_{-0.19}$	$7.52^{+0.16}_{-0.10}$
$0.35 \le z < 0.65$	34	-0.02 ± 0.03	0.44 ± 0.04	$8.33^{+0.13}_{-0.19}$	$7.62^{+0.13}_{-0.10}$
$0.65 \le z < 1.10$	42	$+0.08 \pm 0.03$	0.62 ± 0.05	$8.30^{+0.10}_{-0.10}$	$7.69^{+0.10}_{-0.10}$

which is significant at $\sim 2.7\sigma$ level assuming Gaussian statistics. A similar correlation is seen for our entire sample with $r_k = 0.2$ and null probability $p_{\rm null} = 0.0007$ where we include the upper limits as censored data points and perform survival analysis using the 'CENKEN' function in the 'NADA' package of R. This suggests that the redshift evolution of nebular line ratio in [O II]-detected Mg II systems follows the trend shown by the field galaxies. However, we do not find any correlation between [O III]/H β line ratio and z with $r_k = -0.008, -0.02$ and $p_{\rm null} = 0.87, 0.77$ for the entire sample as well for the clear detections.

Next, we compute the average line ratio using the composite spectrum obtained for the systems with [O II] detections in SDSS-DR12. To generate the composite spectrum, an individual spectrum is shifted to the rest frame of the Mg II absorber while conserving the flux and rebinning on to a same logarithmic scale of a pixel to wavelength used in the SDSS (Bolton et al. 2012). Each spectrum is subtracted with the best-fitting principle component analysis continuum model of Bolton et al. (2012) and the residual spectra are combined together using a median statistics (see also Joshi et al. 2017). Note that, for most of the Mg II systems detected in emission, with redshift range of 0.4–1.1, the [O III] and H β lines fall in the region affected by poorly subtracted sky emission lines. Therefore, to avoid any contamination from sky residuals, we have generated two sets of composite spectra by considering the entire sample with upper limits and another with excluding the systems with upper limits for [O III]. We divide our sample into two redshift bins of 0.36–0.65 and 0.65–1.10, consists of about 49 and 74 galaxies per bin in the composite spectra including upper limits. The number of galaxies over the above z-bins reduces to 34 and 42, respectively, if we consider the systems with only clear detections.

The nebular emission line ratios for [O III]/[O II] and [O III]/H β in a stacked spectrum of the systems with clear detections, over various redshift bins are listed in columns 3 and 4 of Table 4. In the stacked spectra of our entire sample, the log ([O III]/[O II]) is found to be evolving from -0.10 ± 0.02 to -0.03 ± 0.02 by 0.07 dex over the redshift range of $0.36 \le z \le 1.0$. In addition, a clear increasing trend of [O III]/[O II] with z is apparent in the stacked spectra where all the emission lines are clearly detected (see Fig. 16, *lower-left panel*). We find a change of $\sim$0.06 dex in [O III]/[O II] which increases from 0.95 ± 0.06 to 1.22 ± 0.09 between the median redshift of z $\sim$0.52 and $\sim$0.76. Using the star-forming galaxies from the High-z Emission Line Survey, Khostovan et al. (2016) have shown that the [O III]/[O II] evolves out to $z \sim 5$ and is best described by a power law of the form [O III]/[O II] $=(0.59 \pm 0.07) \times (1 + z)^{(1.17 \pm 0.24)}$ (see their equation 6). It also shows a similar change of $\sim$0.07 dex in [O III]/[O II] line ratio for the above redshifts. In addition, we measure the [O III]/[O II] and [O III]/H β ratios in a composite spectrum of low-z (i.e. $z < 0.35$) galaxies, detected in the nebular emission lines in fibre spectra of a background quasars without a prior knowledge of the absorption (see e.g. Straka et al. 2015). It is clear from Fig. 16 (*lower-left panel*) that [O III]/[O II] rises by $\sim$0.21 dex between $0.1 \le z \le 1.1$. Similarly, the [O III]/H β is also found to be evolving from 2.25 ± 0.20 to 4.25 ± 0.47 by $\sim$0.27 dex between $0.1 \le z \le 1.1$ (see Table 4). The above trends indicate that the nebular emissions seen in Mg II systems in our sample follow the trends shown by the general population of normal star-forming galaxies.

In a stacking analysis of galaxies between $0.2 < z < 0.6$ from the Smithsonian Hectospec Lensing Survey (SHELS) galaxy redshift survey, Kewley et al. (2015) have studied the [O III]/[O II] and [O III]/H β line ratios as a function of stellar mass bins, derived from the broad-band photometry. They showed that the optical line ratio is also a strong function of stellar mass, where the galaxies with lower stellar masses show higher line ratio (see also Henry et al. 2013; Ly et al. 2014; Hayashi et al. 2015; Ly et al. 2015). The [O III]/[O II] and [O III]/H β in our Mg II systems are found to be similar as seen in the field galaxies with stellar masses in the range $9.2 < \log(M/{\rm M}_\odot) < 9.4$ (Kewley et al. 2015, see their figs 2 and 3).

We measure the gas phase metallicity (Z) and ionization parameter (q) of the ionized nebula using the IZI (inferring metallicity and ionization parameters) code described in Blanc et al. (2015) and assuming the photoionization model results of Levesque, Kewley & Larson (2010). The Z and q for the three z bins are listed in columns 5 and 6 of Table 4. A typical metallicity of Mg II systems over a redshift range of $0.1 \le z \le 1.1$ is found to be subsolar with $\log Z = 8.3$.

In Fig. 16 (*right-hand panel*), we plot the [O III]/[O II] as a function of W_{2796}. We find that the [O III]/[O II] does not depend on the W_{2796}, with Kendall's rank correlation coefficient (r_k) of 0.02 and null probability $p_{\rm null} = 0.62$ in a survival analysis while including the upper limits as censored data points. In addition, no correlation is seen for systems with clear detection with $r_k = -0.07$ and $p_{\rm null} = 0.22$.

4.7 Velocity width of emission and mass of Mg II absorbers

In this section, we study the kinematic properties of Mg II systems in our sample. The velocity widths (deconvolved for the instrumental broadening) of [O II] $\lambda\lambda$3727, 3729 doublet (i.e. $\sigma_{\rm [O\,II]}$) is found in the range of $\sim 17 \pm 16$ to 194 ± 72 km s^{-1} in SDSS-DR7 and 6 ± 11 to 198 ± 91 km s^{-1} in the SDSS-DR12 spectra with an average $\sigma_{\rm [O\,II]}$ of $\sim$ 75 km s^{-1}. This is similar to a typical velocity dispersion found in the SDSS galaxies (Oh et al. 2011). The KS-test does not indicate any differences between the $\sigma_{\rm [O\,II]}$ in SDSS-DR7 and DR12 with $p_{\rm null} = 0.23$. We also measure the velocity shift ($|\Delta v|$) between the absorption and emission redshift for each system. These values are found to be typically $<$70 km s^{-1}. Now we compare the $\sigma_{\rm [O\,II]}$ and ($|\Delta v|$) with the other parameters of the systems.

In panel (a) of Fig. 17, we look for the dependence of $\sigma_{\rm [O\,II]}$ as a function of redshift of the Mg II absorbers. For the systems detected in SDSS-DR7 fibre spectra, a Spearman rank correlation test finds a correlation with r_s(SDSS-DR7) $= 0.41$ and null probability $p_{\rm null} = 0.0008$ (significant at $\sim 3.2\sigma$). However, no such correlation is seen between $\sigma_{\rm [O\,II]}$ and z for the systems detected in SDSS-DR12 with r_s(SDSS-DR12) $= 0.09$ and $p_{\rm null} = 0.3$. For comparison when

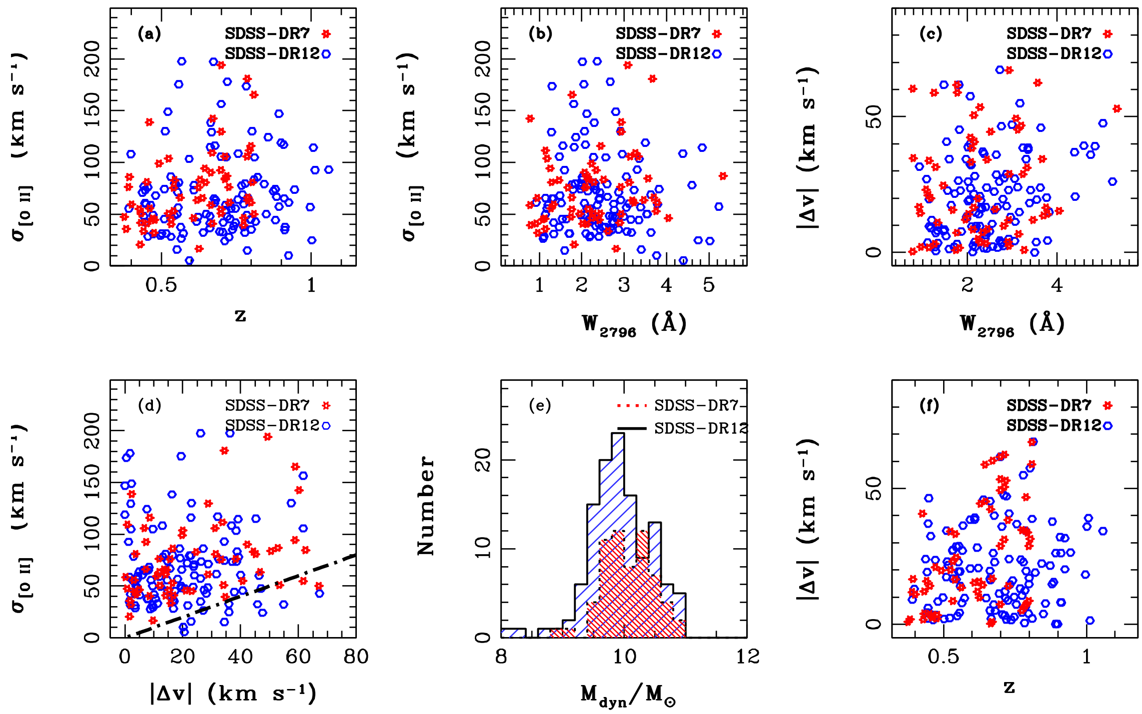

Figure 17. Comparison of the kinematic properties of Mg II absorbers detected in SDSS-DR7(stars) and SDSS-DR12(hexagon) spectra. Panels (a) and (b) show the dependence of velocity widths ($\sigma_{[O\,II]}$) on redshift and the Mg II rest equivalent width (W_{2796}). Panels (c) and (f) show the dependence of the absolute velocity offset ($|\Delta v|$) between the absorption and emission line redshift with W_{2796} and redshift. Panel (d) shows the $\sigma_{[O\,II]}$ as a function of $|\Delta v|$. The dot–dashed line represents the $\sigma_{[O\,II]}=|\Delta v|$ line. Panel (e) shows the distribution of the dynamical mass of Mg II absorbers detected in SDSS-DR7 (dotted histogram) and SDSS-DR12 (solid histogram) spectra.

we use field galaxies from MPA-JHU SDSS-DR7 catalogue, we find no correlation between z and $\sigma_{[O\,II]}$ at $>1.5\sigma$.

In panel (b) of Fig. 17, we compare W_{2796} with $\sigma_{[O\,II]}$. We do not find any correlation between $\sigma_{[O\,II]}$ and W_{2796} of Mg II absorber with a correlation coefficient of r_s(SDSS-DR7) $= -0.11$ and r_s(SDSS-DR12) $= 0.22$ at a significance level of $<2\sigma$. If $\sigma_{[O\,II]}$ can be treated as a proxy to the underlying galaxy mass then the above result suggests that there is no one to one correspondence between W_{2796} and mass of the host galaxy.

We also compare the relative velocity shift ($|\Delta v|$) between absorption and emission line as a function of W_{2796} in panel (c) of Fig. 17. The Spearman rank correlation test finds no correlation at $>2\sigma$ between W_{2796} and $|\Delta v|$ in the SDSS-DR7 and DR12. The maximum $|\Delta v|$ is found to be ~ 70 km s^{-1}. Even though there is no correlation present, it is interesting to note that systems with $W_{2796}>4$ Å have larger $|\Delta v|$. Further, in panel (f) of Fig. 17 we show the dependence of $|\Delta v|$ on redshift. For the Mg II systems detected in SDSS-DR7 spectra, the $|\Delta v|$ shows a correlation with z with r_s(SDSS-DR7) $= 0.47$ and $p_{null} = 0.0001$ (significant at 3.6σ). However, no such correlation is seen for the Mg II systems detected in SDSS-DR12 spectra with r_s(SDSS-DR12) $= 0.05$ and $p_{null} = 0.60$.

In panel (d) of Fig. 17, we compare the $\sigma_{[O\,II]}$ with the absolute relative velocity shift ($|\Delta v|$) between absorption and emission line. Note that, it is quite possible that the absorption and emission may come from two different regions of the galaxy. We do not find any correlation between $\sigma_{[O\,II]}$ and $|\Delta v|$. It is clear from the figure that all but 14 systems are well within a regime where gas is bound to the host galaxy, that is, $|\Delta v| \leq \sigma_{[O\,II]}$, shown as *dot–dashed line* in panel (d) of Fig. 17. We note that among the 14 systems where $|\Delta v| > \sigma_{[O\,II]}$, 8 systems belong to the ultrastrong Mg II absorbers, that is, with $W_{2796} \geq 3$ Å. In addition, two systems are having $2.5 \leq W_{2796} < 3.0$ Å and four systems with $1 \leq W_{2796} < 2.5$ Å. As these systems are predominantly ultrastrong Mg II absorbers, they may be produced in the outflows from the galaxies (Nestor et al. 2011; Gauthier 2013). The fraction of ultrastrong Mg II absorbers with $|\Delta v| > \sigma_{[O\,II]}$ is found to be ∼18 per cent (i.e. 8 out of 43 systems). However, these galaxies do not show signatures of high SFR. In order to draw a firm conclusion on winds, we need high-resolution spectra that will resolve the velocity profiles of absorption line (Kacprzak et al. 2013; Ho et al. 2017).

Next, by using the width of [O II] line we measure the dynamical mass (M_{dyn}) of the Mg II absorbers using,

$$M_{dyn} = C\frac{r_{eff}\sigma^2}{G}. \quad (3)$$

Here, C is a geometric correction factor that can vary depending on the assumed shape and orientation of the galaxies, r_{eff} is the effective half-light radius and G is the gravitational constant. We have used $C = 3$, similar to Maseda et al. (2013). The r_{eff} is computed from the scaling relation of r_{eff} versus z for the star-forming galaxies by Paulino-Afonso et al. (2017, see above Section 4.5) at the redshift of Mg II absorber. The distribution of M_{dyn} for the Mg II systems detected in the SDSS-DR7 (*dotted histogram*) and SDSS-DR12 (*solid histogram*) is shown in panel (e) of Fig. 17. The Mg II systems in our sample probe a range of dynamical mass with log $M_{dyn}(M_\odot) = 8.8$–11.0 and 7.9–10.0 with a median of ∼10.0 and ∼9.9 in the SDSS-DR7 and SDSS-DR12, respectively. Note that, the above dynamical masses represent a lower limit on the mass as the measured σ could suffers from finite fibre loss.

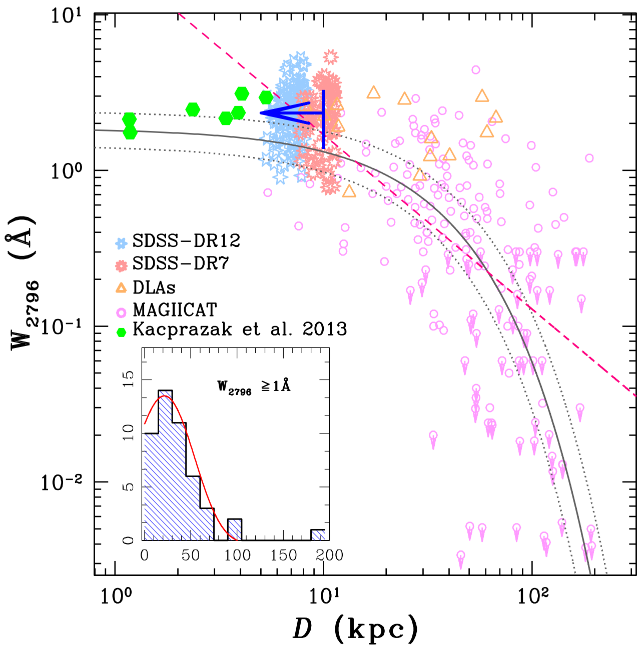

Figure 18. Mg II equivalent width versus impact parameter (ρ) for the systems detected in nebular emission (star). The spectroscopically identified Mg II galaxies from MAGIICAT survey are presented as open circle, whereas those with upper limits on absorption are shown with downward arrows. The hexagons (green) show the seven Mg II galaxies detected at impact parameters of $\leq$ 6 kpc by Kacprzak et al. (2013) at $z < 0.1$. The pink dashed curve is the power-law fit obtained by Chen et al. (2010a). The solid curve is a log-linear maximum likelihood fit given by Nielsen et al. (2013b), while dotted curves provide 1σ uncertainties in the fit. The inset shows the ρ distribution for the Mg II absorbers with W_{2796} $\geq$1 Å. The solid cure represents the skewed Gaussian fit to the ρ distribution.

In summary, we find that the Mg II systems with [O II] emission in our sample share similar properties like normal galaxies with typical line width of ~75 km s^{-1} and dynamical mass of log $M_{\rm dyn}$(M$_\odot$) ~9.9. In addition, most of the absorbers seem to be bound to the host galaxy.

4.8 W_{2796} versus impact parameter

It has been firmly established that the rest-frame equivalent width of Mg II absorption is anticorrelated with the impact parameter, ρ (Bergeron & Boissé 1991; Steidel 1995; Chen et al. 2010a; Rao et al. 2011; Nielsen et al. 2013a,b), albeit with a large scatter. Recently, using a sample of 182 galaxies having impact parameters of $\rho \geq$ 10 kpc, Nielsen et al. (2013a,b) have shown a 7.9σ anticorrelation between W_{2796} and ρ which is well represented by a log-linear relation of logW_{2796}= $(-0.015 \pm 0.002) \times \rho + (0.27 \pm 0.11)$. However, a considerable scatter is seen in the data which may be related to the galaxy luminosity, where more luminous galaxies have larger W_{2796} at a fixed ρ (see Churchill et al. 2013; Nielsen et al. 2013b). Furthermore, using ~7 spectroscopically confirmed low-redshift ($z \sim 0.1$) galaxies, Kacprzak et al. (2013) have shown that anticorrelation between W_{2796} and ρ is maintained even at low-impact parameter of $\leq$ 6 kpc.

Here, we explore the W_{2796} versus ρ correlation at low-impact parameters over a large redshift range of $0.3 \leq z_{\rm abs} \leq 1.1$. Note that, for the Mg II systems at $0.3 \leq z_{\rm abs} \leq 1.1$, the fibre diameter of 3 and 2 arcsec ensures a close star-forming galaxy within an impact parameter of 8.1–12.3 and 5.4−8.2 kpc, respectively. In Fig. 18, we show the distribution of W_{2796} and ρ for our sample in the W_{2796}–ρ plane. The circle and upper limits are for the absorbers and non-absorbers from the spectroscopically identified galaxies hosting Mg II absorbers compiled in the MAGIICAT (Nielsen et al. 2013a,b). We also show a best-fitting power law from Chen et al. (2010a), as a *dashed* curve. At a fixed impact parameter of ~5 and 10 kpc, the above log-linear relation by Nielsen et al. (2013a) predicts a W_{2796} of $1.6^{+0.49}_{-0.38}$ and $1.32^{+0.46}_{-0.34}$ Å. Whereas, at these impact parameters the power-law fit from Chen et al. (2010a) predicts a W_{2796} of $2.9^{+1.7}_{-1.1}$ and $1.3^{+0.9}_{-0.5}$ Å, respectively. The median W_{2796} probed in our sample is found to be 2.23 and 2.32 Å for SDSS-DR7 and SDSS-DR12 data sets, respectively. It is clear from Fig. 18 that majority of the points lie above the log-linear relation of W_{2796} versus ρ.

Next, we estimate the average W_{2796} of Mg II systems expected in our case by assuming the above two functional forms for W_{2796}–ρ relation and associating an impact parameter dependent detection probability of Mg II systems as

$$\langle W_{2796}\rangle = \frac{\int_0^{\rho_{\rm max}} W(\rho)p(\rho){\rm d}\rho}{\int_0^{\rho_{\rm max}} p(\rho){\rm d}\rho}. \quad (4)$$

Here, $W(\rho)$ is W_{2796}–ρ relation, $\rho_{\rm max}$ is the maximum impact parameter, taken as a projected fibre radius of 10 kpc at a median redshift of 0.65 for the 3 arcsec SDSS-DR7 fibre. $p(\rho)$ is impact parameter dependent detection probability of Mg II absorber, which is defined as $p(\rho) = \int_0^{\rho} 2\pi\rho{\rm d}\rho/\pi\rho^2_{\rm max}$, assuming a spherical halo. Using equation (4) and the best-fitting log-linear and power-law relations for W_{2796}–ρ, we find an average W_{2796} up to $\rho \sim$ 10 kpc to be $1.4^{+0.6}_{-0.4}$ and $2.1^{+0.4}_{-0.3}$ Å, respectively. However, if we consider the impact parameter corresponding to a 2 arcsec fibre used in SDSS-DR12 at median redshift, that is, of ~ 7 kpc, the W_{2796} for above two models are found to be $1.6^{+0.5}_{-0.4}$ and $3.2^{+0.5}_{-0.4}$ Å. The median value found for our sample, while consistent with these average values within 2σ, is closer to the power-law prediction.

Furthermore, using the ρ distribution of spectroscopically confirmed strong, W_{2796} $\geq$1 Å, Mg II absorbers from MAGIICAT (i.e. ~ 40 systems) along with the seven systems from Kacprzak et al. (2013), we computed the detection probability of strong Mg II absorbers within impact parameter of $\leq$ 8 kpc (a typical projected size of SDSS fibre). The distribution of the ρ is shown in the inset of Fig. 18. We have modelled the ρ distribution with a skewed Gaussian (see the *solid curve* in Fig. 18) and compute the probability of strong absorbers being less than 8 kpc to be ~11 per cent. The detection probability further increases to ~25 per cent if we consider the systems with W_{2796} $\geq$2 Å. Recall that, about 95 per cent of strong Mg II systems in our sample do not have [O II] nebular emission detected in SDSS fibres above the detection threshold. Therefore, the above larger probability of strong Mg II absorber being at smaller ρ ($\leq$8 kpc) than the ~1–3 per cent detection rate of nebular emission lines from Mg II absorbers (see Fig. 9) either related to large intrinsic spread in ρ at a given W_{2796} or a large spread in $L_{\rm [O\,II]}$ at a given W_{2796}.

5 CONCLUSIONS

Using the Mg II absorbers found in SDSS-DR7 and SDSS-DR12 spectra, we have complied a sample of ~198 Mg II systems with detectable nebular emission lines over a redshift range of $0.36 \leq z_{\rm abs} \leq 1.1$. By studying the absorption and emission line properties of this unique set of Mg II systems, we derive the following results.

(1) The Mg II absorbers in our sample are found to be mostly sub-$L^\star$ with luminosities ranging from 0.14 to 3.5 $L^\star_{\rm [O\,II]}$ and 0.09 to

3.5 $L^{\star}_{[\mathrm{O\,II}]}$, with a median of 0.54 and 0.43 $L^{\star}_{[\mathrm{O\,II}]}$ in the SDSS-DR7 and SDSS-DR12, respectively. A typical SFR of the Mg II systems uncorrected for dust reddening and fibre losses is found to be in the range of 0.5−20 $M_{\odot}$ yr^{-1}. We show that our data suffer from finite fibre size effects and all the above-quoted values should be considered as lower limits.

(2) The nebular emission is preferentially detected in the strong Mg II systems, that is, ∼ 96 per cent of systems are having $W_{2796} \geq 1$ Å, with a mean W_{2796} of ∼ 2.3 Å. The detection rate of nebular emission from Mg II absorbers with $W_{2796} > 2$ Å and $L_{[\mathrm{O\,II}]} \geq 0.3\,L^{\star}$ is found to be very small at 3 per cent and 1 per cent in the SDSS-DR7 and DR12 spectra, respectively. We find the detection probability to depend on the W_{2796}, where larger W_{2796} systems show higher detection rate. Furthermore, the detection rate increases with the size of the fibre aperture (see Fig. 9). For a given W_{2796}, the detection rate of nebular emission increases with increasing z.

(3) In contrast to the strong correlation seen between W_{2796} and $\Sigma_{[\mathrm{O\,II}]}$ obtained from the stacked spectra, our Mg II systems with nebular emission do not show any statistically significant correlation between $\Sigma_{[\mathrm{O\,II}]}$ and W_{2796} even when we restrict ourselves to narrow z ranges. We conclude that the correlation observed in the stacked spectra is dominated by the increase in nebular line detection probability with W_{2796}. In addition, we find that $\Sigma_{[\mathrm{O\,II}]}$ is strongly correlated with redshift. This is also dominated by the fibre size effect where at higher redshifts the projected size of the fibres will cover a larger fraction of galaxy area than for galaxies at low redshifts.

(4) We have found that the physical conditions in galaxies in our sample evolve with redshift. A rise of ∼0.2 dex in the nebular emission line ratio of [O III]/[O II] and [O III]/Hβ is seen over a redshift range of $0.1 \leq z \leq 1$. This is similar to what is seen in normal galaxies at this redshift range. From the well-known stellar mass dependence on the line ratio, we suggest that the Mg II absorbers likely belong to the population of low-stellar mass galaxies with a typical stellar masses in the range $9.2 < \log(M/\mathrm{M}_{\odot}) < 9.4$.

(5) The typical velocity widths ($\sigma_{[\mathrm{O\,II}]}$) of the [O II] nebular emission in Mg II absorbers are found in the range of 6–198 km s^{-1}, with an average $\sigma_{[\mathrm{O\,II}]}$∼75 km s^{-1}. The $\sigma_{[\mathrm{O\,II}]}$ does not show any correlation with z and W_{2796}. We measure the maximum relative velocity shift ($|\Delta v|$) between emission and absorption to be ∼70 km s^{-1}. By comparing the $\sigma_{[\mathrm{O\,II}]}$ and $|\Delta v|$, we show that most systems are well within the regime where gas is bound to the host galaxy. In addition, the Mg II absorbers probe the galaxies with range of dynamical mass, that is, $\log M_{\mathrm{dyn}}(\mathrm{M}_{\odot}) = 7.5$–10.8.

(6) We show that Mg II systems follow the well-known relationships between W_{2796} and impact parameter even at small impact parameters. A comparison of their W_{2796} distribution with that of the MW shows that the GOTOQs are most likely produced in the ISM+halo of their host galaxy. Hence, these systems are ideally suited for probing various feedback processes at play in $z < 1$ galaxies. In addition, by comparing the DR and R parameters of strong Mg II absorbers with and without emission line detection, we find that most of the GOTOQs have large R values and DR ∼ 1. Therefore, good fraction of these systems could be DLAs.

ACKNOWLEDGEMENTS

RS, PN and PPJ acknowledge the support from Indo-French Centre for the Promotion of Advance Research (IFCPAR) under project number 5504-2. We thank the anonymous referee for constructive comments and suggestions.

Funding for the Sloan Digital Sky Survey IV has been provided by the Alfred P. Sloan Foundation, the U.S. Department of Energy Office of Science, and the Participating Institutions. SDSS-IV acknowledges support and resources from the Center for High-Performance Computing at the University of Utah. The SDSS web site is www.sdss.org.

SDSS-IV is managed by the Astrophysical Research Consortium for the Participating Institutions of the SDSS Collaboration including the Brazilian Participation Group, the Carnegie Institution for Science, Carnegie Mellon University, the Chilean Participation Group, the French Participation Group, Harvard-Smithsonian Center for Astrophysics, Instituto de Astrofísica de Canarias, The Johns Hopkins University, Kavli Institute for the Physics and Mathematics of the Universe (IPMU)/University of Tokyo, Lawrence Berkeley National Laboratory, Leibniz Institut für Astrophysik Potsdam (AIP), Max-Planck-Institut für Astronomie (MPIA Heidelberg), Max-Planck-Institut für Astrophysik (MPA Garching), Max-Planck-Institut für Extraterrestrische Physik (MPE), National Astronomical Observatories of China, New Mexico State University, New York University, University of Notre Dame, Observatário Nacional/MCTI, The Ohio State University, Pennsylvania State University, Shanghai Astronomical Observatory, United Kingdom Participation Group, Universidad Nacional Autónoma de México, University of Arizona, University of Colorado Boulder, University of Oxford, University of Portsmouth, University of Utah, University of Virginia, University of Washington, University of Wisconsin, Vanderbilt University and Yale University.

REFERENCES

Abazajian K. N. et al., 2009, ApJS, 182, 543
Alam S. et al., 2015, ApJS, 219, 12
Bahcall J. N. et al., 1993, ApJS, 87, 1
Baldwin J. A., Phillips M. M., Terlevich R., 1981, PASP, 93, 5
Barton E. J., Cooke J., 2009, AJ, 138, 1817
Bergeron J., 1986, A&A, 155, L8
Bergeron J., Boissé P., 1991, A&A, 243, 344
Blanc G. A., Kewley L., Vogt F. P. A., Dopita M. A., 2015, ApJ, 798, 99
Bolton J., Meiksin A., White M., 2004, MNRAS, 348, L43
Bolton A. S. et al., 2012, AJ, 144, 144
Bordoloi R. et al., 2011, ApJ, 743, 10
Bordoloi R. et al., 2014, ApJ, 794, 130
Borthakur S., Tripp T. M., Yun M. S., Momjian E., Meiring J. D., Bowen D. V., York D. G., 2010, ApJ, 713, 131
Bouché N., Murphy M. T., Péroux C., Csabai I., Wild V., 2006, MNRAS, 371, 495
Bouché N., Murphy M. T., Péroux C., Davies R., Eisenhauer F., Förster Schreiber N. M., Tacconi L., 2007, ApJ, 669, L5
Chelouche D., Bowen D. V., 2010, ApJ, 722, 1821
Chen H.-W., Helsby J. E., Gauthier J.-R., Shectman S. A., Thompson I. B., Tinker J. L., 2010a, ApJ, 714, 1521
Chen H.-W., Wild V., Tinker J. L., Gauthier J.-R., Helsby J. E., Shectman S. A., Thompson I. B., 2010b, ApJ, 724, L176
Churchill C. W., Mellon R. R., Charlton J. C., Jannuzi B. T., Kirhakos S., Steidel C. C., Schneider D. P., 2000, ApJS, 130, 91
Churchill C. W., Trujillo-Gomez S., Nielsen N. M., Kacprzak G. G., 2013, ApJ, 779, 87
Comparat J. et al., 2016, MNRAS, 461, 1076
Dutta R., Srianand R., Gupta N., Joshi R., Petitjean P., Noterdaeme P., Ge J., Krogager J.-K., 2017, MNRAS, 465, 4249
Gauthier J.-R., 2013, MNRAS, 432, 1444
Gupta N., Srianand R., Petitjean P., Bergeron J., Noterdaeme P., Muzahid S., 2012, A&A, 544, A21
Hayashi M. et al., 2015, PASJ, 67, 80
Henry A., Martin C. L., Finlator K., Dressler A., 2013, ApJ, 769, 148

Herenz P., Richter P., Charlton J. C., Masiero J. R., 2013, A&A, 550, A87
Hewett P. C., Irwin M. J., Bunclark P., Bridgeland M. T., Kibblewhite E. J., He X. T., Smith M. G., 1985, MNRAS, 213, 971
Ho S. H., Martin C. L., Kacprzak G. G., Churchill C. W., 2017, ApJ, 835, 267
Joshi R., Srianand R., Noterdaeme P., Petitjean P., 2017, MNRAS, 465, 701
Kacprzak G. G., Churchill C. W., Steidel C. C., Murphy M. T., 2008, AJ, 135, 922
Kacprzak G. G., Churchill C. W., Ceverino D., Steidel C. C., Klypin A., Murphy M. T., 2010, ApJ, 711, 533
Kacprzak G. G., Churchill C. W., Evans J. L., Murphy M. T., Steidel C. C., 2011, MNRAS, 416, 3118
Kacprzak G. G., Churchill C. W., Steidel C. C., Spitler L. R., Holtzman J. A., 2012, MNRAS, 427, 3029
Kacprzak G. G., Cooke J., Churchill C. W., Ryan-Weber E. V., Nielsen N. M., 2013, ApJ, 777, L11
Kennicutt R. C., Jr, 1998, ApJ, 498, 541
Kewley L. J., Dopita M. A., Sutherland R. S., Heisler C. A., Trevena J., 2001, ApJ, 556, 121
Kewley L. J., Zahid H. J., Geller M. J., Dopita M. A., Hwang H. S., Fabricant D., 2015, ApJ, 812, L20
Khostovan A. A., Sobral D., Mobasher B., Smail I., Darvish B., Nayyeri H., Hemmati S., Stott J. P., 2016, MNRAS, 463, 2363
Lanzetta K. M., Bowen D., 1990, ApJ, 357, 321
Levesque E. M., Kewley L. J., Larson K. L., 2010, AJ, 139, 712
López G., Chen H.-W., 2012, MNRAS, 419, 3553
Lundgren B. F. et al., 2012, ApJ, 760, 49
Ly C., Malkan M. A., Nagao T., Kashikawa N., Shimasaku K., Hayashi M., 2014, ApJ, 780, 122
Ly C., Rigby J. R., Cooper M., Yan R., 2015, ApJ, 805, 45
Martin C. L., Bouché N., 2009, ApJ, 703, 1394
Martin C. L., Shapley A. E., Coil A. L., Kornei K. A., Bundy K., Weiner B. J., Noeske K. G., Schiminovich D., 2012, ApJ, 760, 127
Maseda M. V. et al., 2013, ApJ, 778, L22
Ménard B., Chelouche D., 2009, MNRAS, 393, 808
Ménard B., Wild V., Nestor D., Quider A., Zibetti S., Rao S., Turnshek D., 2011, MNRAS, 417, 801
Nakajima K., Ouchi M., 2014, MNRAS, 442, 900
Nestor D. B., Johnson B. D., Wild V., Ménard B., Turnshek D. A., Rao S., Pettini M., 2011, MNRAS, 412, 1559
Nielsen N. M., Churchill C. W., Kacprzak G. G., Murphy M. T., 2013a, ApJ, 776, 114
Nielsen N. M., Churchill C. W., Kacprzak G. G., 2013b, ApJ, 776, 115
Noterdaeme P., Srianand R., Mohan V., 2010, MNRAS, 403, 906
Oh K., Sarzi M., Schawinski K., Yi S. K., 2011, ApJS, 195, 13
Osterbrock D. E., Ferland G. J., 2006, Astrophysics of Gaseous Nebulae and Active Galactic Nuclei, 2nd edn. University Science Books, Mill Valley, CA
Pâris I. et al., 2012, A&A, 548, A66
Paulino-Afonso A., Sobral D., Buitrago F., Afonso J., 2017, MNRAS, 465, 2717
Petitjean P., Bergeron J., 1990, A&A, 231, 309
Rao S. M., Turnshek D. A., 2000, ApJS, 130, 1
Rao S. M., Turnshek D. A., Nestor D. B., 2006, ApJ, 636, 610
Rao S. M., Belfort-Mihalyi M., Turnshek D. A., Monier E. M., Nestor D. B., Quider A., 2011, MNRAS, 416, 1215
Rao S. M., Turnshek D. A., Sardane G. M., Monier E. M., 2017, preprint (arXiv:1704.01634)
Richter P., 2012, ApJ, 750, 165
Rigby J. R., Charlton J. C., Churchill C. W., 2002, ApJ, 565, 743
Rubin K. H. R., Prochaska J. X., Koo D. C., Phillips A. C., Weiner B. J., 2010, ApJ, 712, 574
Rubin K. H. R., Prochaska J. X., Koo D. C., Phillips A. C., 2012, ApJ, 747, L26
Savage B. D. et al., 2000, ApJS, 129, 563
Srianand R., 1996, ApJ, 462, 643
Srianand R., Khare P., 1994, ApJ, 428, 82
Steidel C. C., 1995, in Meylan G., ed., QSO Absorption Lines. Springer-Verlag, Berlin, p. 139
Steidel C. C., Kollmeier J. A., Shapley A. E., Churchill C. W., Dickinson M., Pettini M., 2002, ApJ, 570, 526
Steidel C. C. et al., 2014, ApJ, 795, 165
Straka L. A. et al., 2015, MNRAS, 447, 3856
Tremonti C. A., Moustakas J., Diamond-Stanic A. M., 2007, ApJ, 663, L77
Tripp T. M., Jenkins E. B., Bowen D. V., Prochaska J. X., Aracil B., Ganguly R., 2005, ApJ, 619, 714
Weiner B. J. et al., 2009, ApJ, 692, 187
Wild V., Hewett P. C., Pettini M., 2007, MNRAS, 374, 292
York D. G. et al., 2012, MNRAS, 423, 3692
Zhu G., Ménard B., 2013, ApJ, 770, 130

SUPPORTING INFORMATION

Supplementary data are available at *MNRAS* online.

Table 2. Sample of Mg II absorbers with nebular emission line.

Please note: Oxford University Press is not responsible for the content or functionality of any supporting materials supplied by the authors. Any queries (other than missing material) should be directed to the corresponding author for the article.

This paper has been typeset from a TEX/LATEX file prepared by the author.